Ocean Modelling 124 (2018) 94–110

Contents lists available at ScienceDirect

Ocean Modelling

journal homepage: www.elsevier.com/locate/ocemod

FVCOM one-way and two-way nesting using ESMF: Development and validation

Jianhua Qi[a,*], Changsheng Chen[a,c,d], Robert C. Beardsley[b]

[a] School for Marine Science and Technology, University of Massachusetts Dartmouth, New Bedford, MA 02744, USA
[b] Department of Physical Oceanography, Woods Hole Oceanographic Institution, Woods Hole, MA 02543, USA
[c] International Center for Marine Studies, Shanghai Ocean University, Shanghai, PR China
[d] College of Atmospheric Sciences, Sun Yat-Sen University, Guangzhou, PR China

ARTICLE INFO

Keywords:
FVCOM ocean model
ESMF
One-way nesting
Two-way nesting

ABSTRACT

Built on the Earth System Modeling Framework (ESMF), the one-way and two-way nesting methods were implemented into the unstructured-grid Finite-Volume Community Ocean Model (FVCOM). These methods help utilize the unstructured-grid multi-domain nesting of FVCOM with an aim at resolving the multi-scale physical and ecosystem processes. A detail of procedures on implementing FVCOM into ESMF was described. The experiments were made to validate and evaluate the performance of the nested-grid FVCOM system. The first was made for a wave-current interaction case with a two-domain nesting with an emphasis on qualifying a critical need of nesting to resolve a high-resolution feature near the coast and harbor with little loss in computational efficiency. The second was conducted for the pseudo river plume cases to examine the differences in the model-simulated salinity between one-way and two-way nesting approaches and evaluate the performance of mass conservative two-way nesting method. The third was carried out for the river plume case in the realistic geometric domain in Mass Bay, supporting the importance for having the two-way nesting for coastal-estuarine integrated modeling. The nesting method described in this paper has been used in the Northeast Coastal Ocean Forecast System (NECOFS)-a global-regional-coastal nesting FVCOM system that has been placed into the end-to-end forecast and hindcast operations since 2007.

1. Introduction

The primitive equation numerical ocean models are valuable tools for understanding the complexities of the ocean's physical state, biophysical interaction, and their long-term changes due to natural and anthropogenic factors. In the past few decades, benefiting from the emergence of the supercomputer systems and the high-performance computing (HPC) techniques, many global ocean models have been developed for the study of climate. The popular global models include MOM (Modular Ocean Model) (Pacanowski and Griffies, 1999); OPA (Océan PArallélisé) (Madec et al., 1998); POP (Parallel Ocean Program) (Smith et al., 1999); MIT-GCM (Marshall et al., 1997a,b), and the HYCOM (Hybrid Coordinate Ocean Model) (Bleck, 2002; Chassignet et al., 2003, 2006). Coupled with atmospheric climate models, these ocean models have enhanced our understanding of the impact of climate change on the ocean environment on global-to-basin scales and the role of oceanic processes in global and regional climate change.

All of these models, however, are constructed with structured grids, which limit their ability to adequately resolve smaller-scale processes and their interaction with the large-scale circulation. It is a major challenge for a global ocean model to resolve the multi-scale processes relevant to global climate and to capture the correct physics of vertical and lateral mixing. Complexity of the earth system models and the necessity to perform long-term (>100 years) integrations will always dictate limitations on vertical and horizontal resolution in the model components. With typical spatial resolution of about 100 km (IPCC, 2007), commonly-used structured-grid ocean global models do not adequately resolve smaller scale climatologically important oceanic processes, especially in the coastal and shelf regions, straits and channels, and regions with complex bottom topography.

Grid refinement techniques, such as nesting, conjoined grids and adaptive grids, could be employed to endow ocean models with variable resolution capabilities, and to permit these models to better resolve multi-scale processes in global and regional simulations. One-way or two-way nesting is a common approach used in both atmosphere and ocean models (Fox and Maskell, 1995; Sheng et al., 2005; Debreu and Blayo, 2008; Debreu et al., 2012; Chen et al., 2013a,b, 2016; Chen and Beardsley, 2015; Zhang et al., 2016a,b). The nesting approach needs to

* Corresponding author.
E-mail addresses: jqi@umassd.edu (J. Qi), c1chen@umassd.edu (C. Chen).

https://doi.org/10.1016/j.ocemod.2018.02.007
Received 24 July 2017; Received in revised form 22 February 2018; Accepted 28 February 2018
Available online 05 March 2018
1463-5003/

enforce mass and energy conservation at the seam where two different-size grids are connected. This approach is, however, fraught with problems (Debreu and Blayo, 2008; Chen and Beardsley, 2015; Chen et al., 2016). For example, in a free-surface shallow-water ocean model, under a long-wave approximation, the discrete equation makes non-dispersive surface gravity waves become dispersive. Since the numerical dispersion depends on horizontal resolution, the different grid sizes of the two domains at the nesting boundary can cause a jump of the model-computed phase and group speeds. For a structured-grid model, a numerical treatment is then required to disperse inconsistent energy exchange between the two grids, and to ensure mass and energy conservation at the nesting boundary. Analogous baroclinic dynamics face the same issue. This treatment usually works for a short-term simulation but needs to be tested for the long time-scale simulations generally used in climate studies.

Unlike the structured-grid nesting, unstructured-grid nesting is much simpler. By linking two domains with common cells, this approach produces the same surface gravity features at the boundary, which ensures volume and mass conservation between the two domains (Chen et al., 2013b, 2016). This approach also makes it practical to resolve multi-scale processes in the ocean. For example, energetic high-frequency internal waves are frequently generated over submarine banks, seamounts, and ridges. We can create a finer grid over those regions and nest it to the regional model. In this small sub-domain, we can turn on the non-hydrostatic dynamics in the sub-domain and then hydrostatic dynamics in the regional domain. Using the varying-size grids to specify the nested boundary with coarser grids in the region where the hydrostatic dynamics are dominant, we can run the multi-scale coupling with an unstructured-grid model in a more computational efficient way. The key reason for implementing the nesting method into FVCOM is to efficiently run a model on a supercomputer by running larger and smaller domain models simultaneously on different processors with data exchange through boundaries. This approach could overcome the shortcoming of the model running efficiency that is restricted by the time step as the grid is refined.

FVCOM is a prognostic, unstructured-grid, Finite-Volume, free-surface, 3-D primitive equation Coastal Ocean Model, which was originally developed by Chen et al. (2003) and improved and upgraded by community efforts (Chen et al., 2006, 2013a). The equations are cast in a generalized terrain-following coordinate system with spatially variable vertical distribution (Pietrzak et al., 2002). In the horizontal, the equations are discretized using non-overlapped triangular grids, which provide accurate fitting of irregular coastal geometries and flexibility in refining the grid over steep continental margins, ridges, and around islands. The spatial fluxes of momentum are discretized using a second-order accurate finite-volume method (Kobayashi et al., 1999). A flux formulation for scalars (e.g. temperature, salinity) is used in conjunction with a vertical velocity adjustment to enforce exact conservation of the scalar quantities. A Smagorinsky formulation (Smagorinsky, 1963) is used to parameterize horizontal diffusion and turbulent vertical mixing is calculated using the General Ocean Turbulence Model (GOTM) libraries (Burchard, 2002), with the 2.5 level Mellor and Yamada (1982) turbulence model used as the default. FVCOM is coded for both spherical and Cartesian coordinates and is solved numerically with an option of either a mode-split (like POM and ROMs) or semi-implicit integration method (Lai et al., 2010a,b).

The UMASSD/WHOI research team has recently successfully applied the FVCOM system to resolve and examine global-to-wetland scale ocean processes in the Arctic (Chen et al., 2016; Zhang et al., 2016a, b), the western North Atlantic (Chen et al., 2013b; Beardsley et al., 2013) and the Arabian Gulf-Sea of Oman (Chen and Beardsley, 2015). The FVCOM model has been widely used for estuarine and ocean applications by scientists with users over 38 countries, such as the Mexican Gulf (e.g. Yang et al., 2016; Zheng and Weisberg, 2012), Northeast Pacific (e.g. Foreman et al., 2012; Lin and Fissel, 2014; Peng et al., 2014), the European coastal areas (e.g. Cazenave et al., 2016), the Persian Gulf (e.g. Xue and Eltahir, 2015) and China Sea areas (e.g. Chen et al., 2012), as well as the Great Lakes (e.g. Anderson and Schwab, 2013). The Northeast Coastal Ocean Forecast System (NECOFS) is an integrated atmospheric and ocean forecast and hindcast system built on the multi-scale nested FVCOM framework (http://134.88.228.119:8080/fvcomwms/). Utilizing the flexible grid configuration and simple one-way nesting, this system is capable of resolving realistic global and coastal tides, stratification and multi-scale subtidal flows down to wetland inundation and drying. The one-way nesting used in NECOFS was achieved by an offline approach, which required to be done with two steps. First, run the larger domain model and output the variables at the nodes and cell centroids on the common nesting boundaries. Second, run the smaller domain model with the boundary conditions provided by the larger domain model. This approach is generally sound, but cannot efficiently use the supercomputer computational nodes by running larger and smaller domain models simultaneously with boundary conditions exchange.

Over the past decade, an emphasis on integrated multi-component modeling has emerged: reflecting an increase in scientific capabilities and computing capacity, and resulting in several ambitious, coupled Earth system modeling efforts. Among them, there are several efforts funded by federal agencies, including NOAA, NASA, NSF and DOE. Two examples are ESMF (Hill et al., 2004; Collins et al., 2005; Dunlap et al., 2008) and the Model Coupling Toolkit (MCT) (Larson et al., 2005; Jacob et al., 2005). Several other generic component-based coupling software tools include the Common Component Architecture (CCA) (Bernholdt et al., 2006; McInnes et al., 2006) and the domain science specific coupling components and framework (e.g. Ecosystem Modeling, Space Weather Modeling Framework) (Wang et al., 2011). ESMF defines architecture for composing complex, coupled modeling systems and includes data structures and utilities for developing individual models. The basic idea behind ESMF is that complicated applications should be broken up into smaller pieces, or components. A component is a unit of software composition that has a coherent function and a standard calling interface and behavior. Components can be assembled to create multiple applications, and different implementations of a component may be available. In ESMF, a component may be a physical domain, or a function such as a coupler or I/O system. ESMF also includes toolkits for building components and applications, such as regridding software, calendar management, logging and error handling, and parallel communications (ESMF Joint Specification Team, 2016b). Two models or more, no matter whether or not they are structured grid or unstructured grid, can be coupled in either one-way or two-way framework (Fig. 1).

We have implemented FVCOM into ESMF. This paper was written to first describe the ESMF-FVCOM framework and then present the validation results from numerical experiments done under idealized and realistic forcing cases. The validation experiments were made with an aim at not only evaluating performance of the FVCOM nesting on the ESMF framework but also highlighting the critical needs for a two-way nesting to resolve the realistic physics in a multi-scale coastal ocean system. The domain nesting algorithms developed in this work could significantly improve multi-domain coupling for ocean applications.

The remaining sections of the paper are organized as follows. In Section 2, the methodology of FVCOM one-way and two-way nesting on the ESMF framework is described. In Section 3, an experiment made to evaluate the performance of the nesting method for a fully current-wave coupled FVCOM system in the Northeast U.S. coastal region is presented. In Section 4, the two-way nesting method is discussed through the experiments first with the pseudo river plume cases and then with a realistic geometric Mass coastal river plume case. In Section 5, the conclusions are summarized.

2. FVCOM nesting module developed under the ESMF framework

The FVCOM nesting module was developed under a standard ESMF

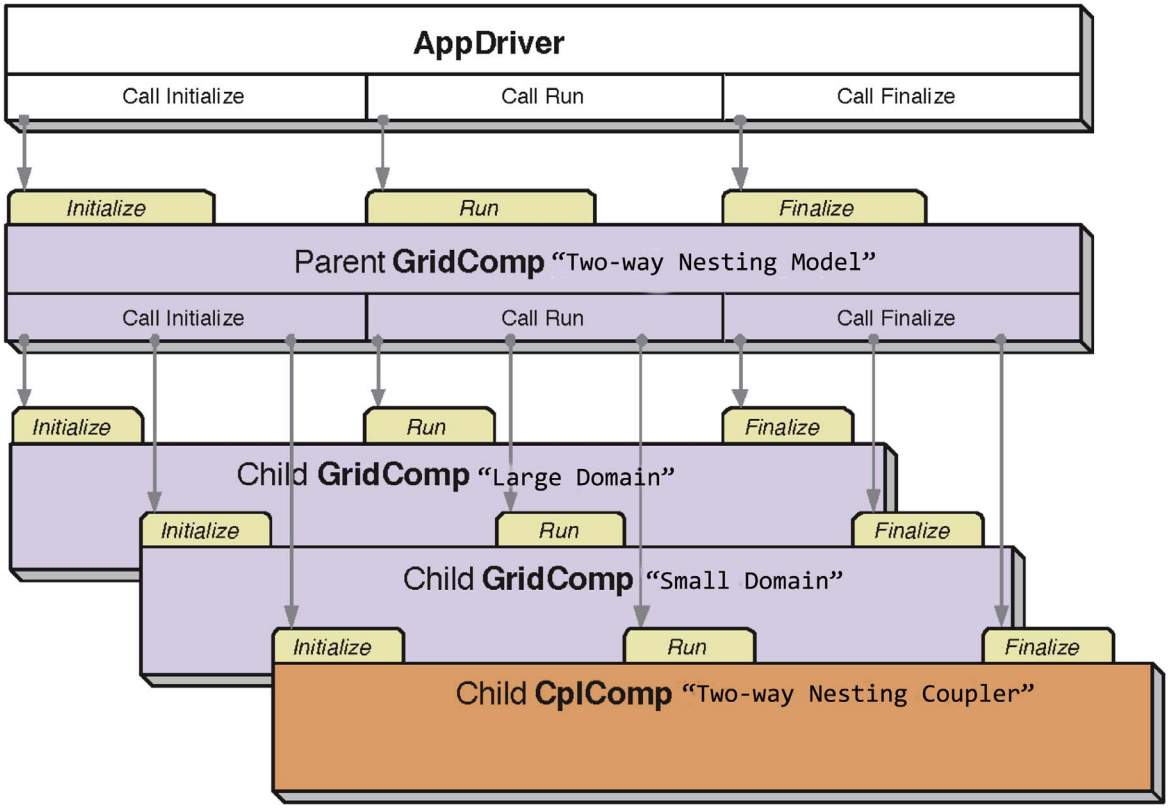

Fig. 1. The diagram of ESMF two-way nesting frame. This figure was drawn by modifying Fig. 2 in ESMF User Guide (ESMF Joint Specification Team, 2016b).

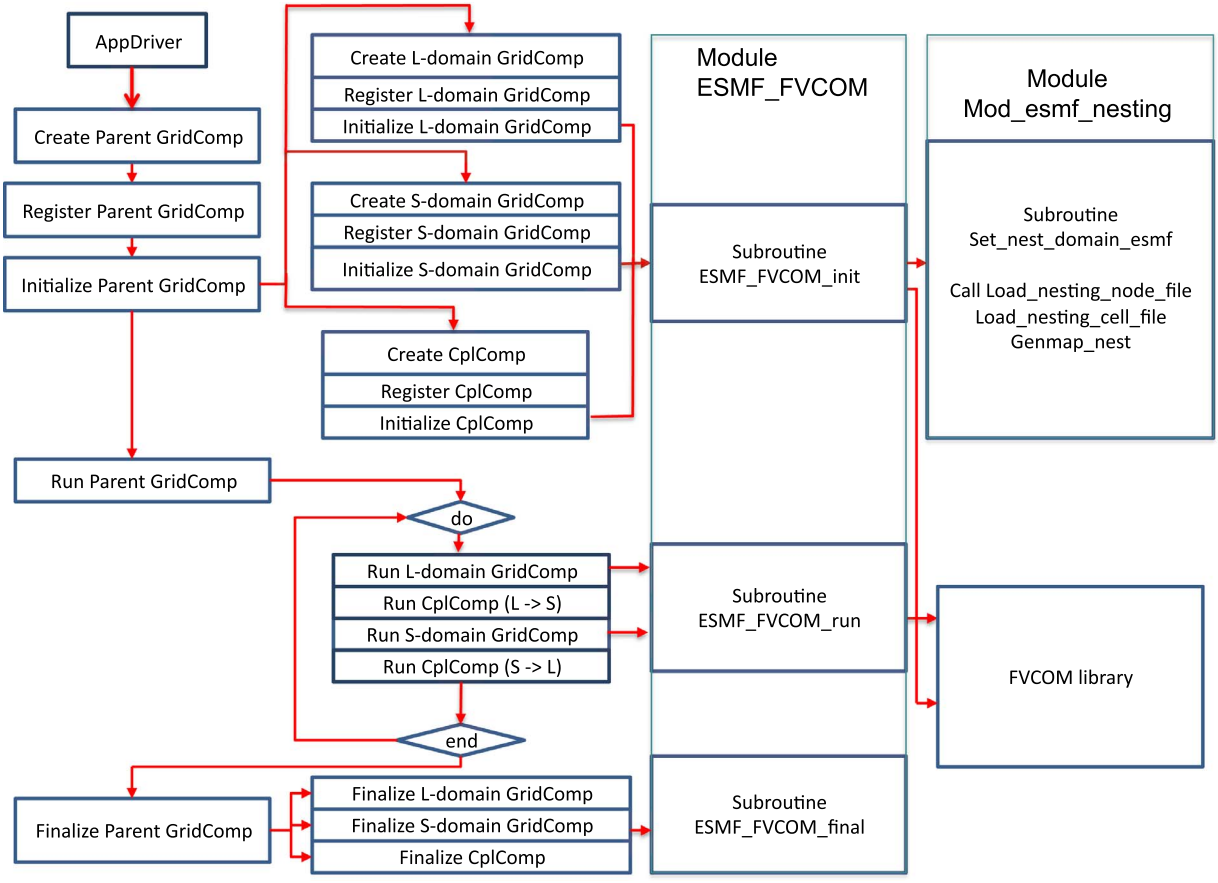

Fig. 2. The flow chart of FVCOM two-way nesting on the ESMF framework.

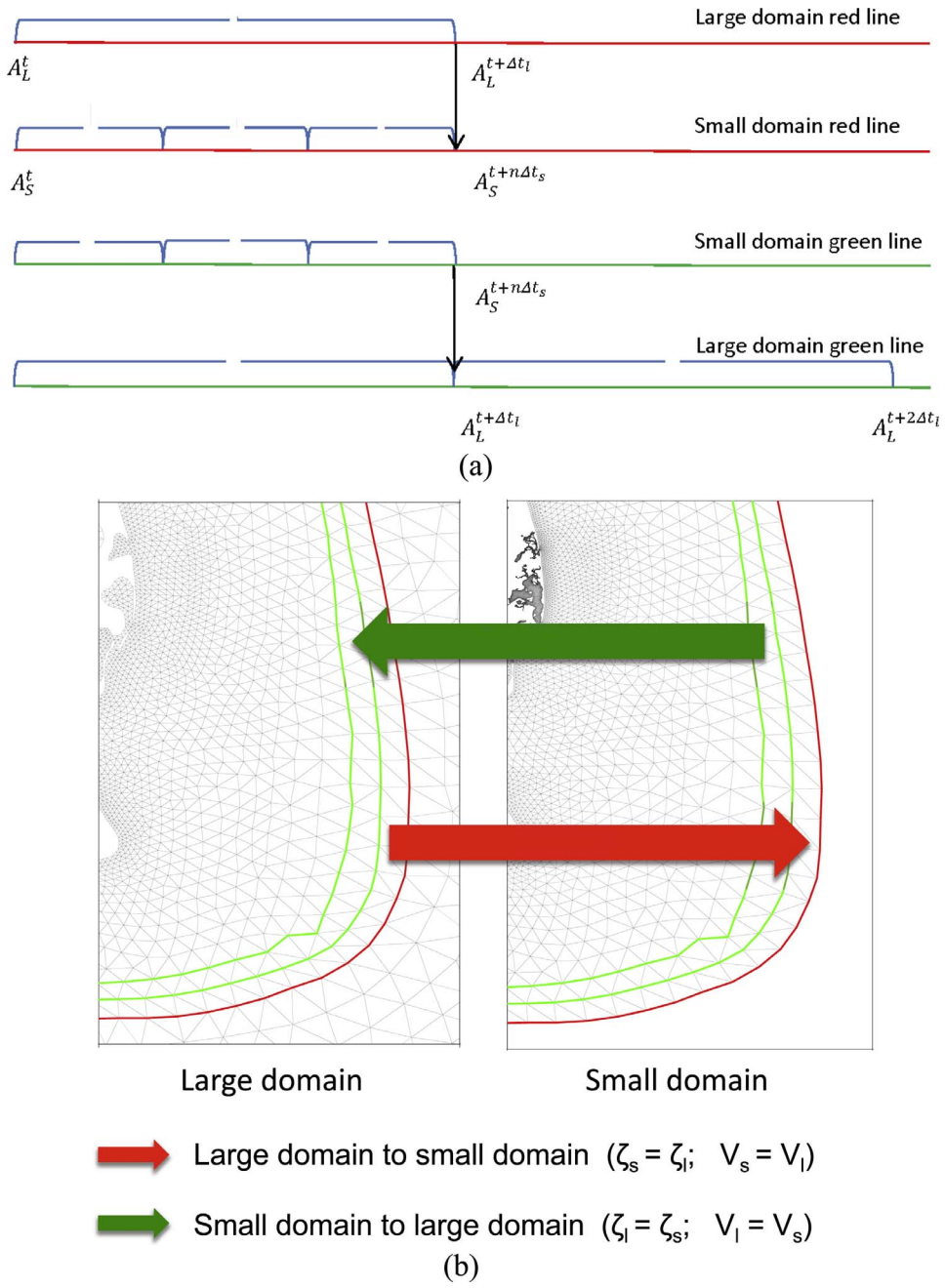

Fig. 3. Illustration of the time integration and data exchange between large and small domains. The red lines in (a) and the red arrow in (b): the data exchange from large domain to small domain. The green lines in (a) and the green arrow in (b): the data exchange from small domain to large domain. (For interpretation of the references to color in this figure legend, the reader is referred to the web version of this article.)

two-way coupling framework. In ESMF, coupling of two models or two domains is composited with components (ESMF Joint Specification Team 2016a), including one parent gridded component, two child gridded components, and a coupler component (Fig. 1). Coupling starts with an application driver, which controls the model system step by step from parent component to child components and coupler component. Each ESMF component contains initialize, run and finalize modules. The application driver calls the initialize module of parent component and then directly goes to call the initialize modules of all child components. The run and finalize modules work in the same way.

Implementing FVCOM into ESMF, for an example of a two-way nesting application, we defined two child gridded components named “Large Domain” and “Small Domain” and one child coupler component named “Two-way Nesting Coupler”. A flow chart is shown in Fig. 2 to illustrate the ESMF-based two-way nesting module in FVCOM. In this chart, the first and second columns are built on the ESMF architecture. The third column is a module named “ESMF_FVCOM”, which is developed on both ESMF and FVCOM architectures to establish the connection between the ESMF framework and FVCOM library. The fourth column includes the FVCOM library with the original FVCOM version 4.0 codes and a module named “Mod_esmf_nesting”. This module is to load node and cell indexes of both large and small domains’ nesting boundaries. It is also used to generate sub-domain maps of nesting boundaries for parallelization.

The FVCOM library is built for the updated version of the FVCOM source codes with inclusion of wave-current interaction. Both large and small domains use the same FVCOM library. The model simulations of large and small domains are grouped on different amounts of cluster

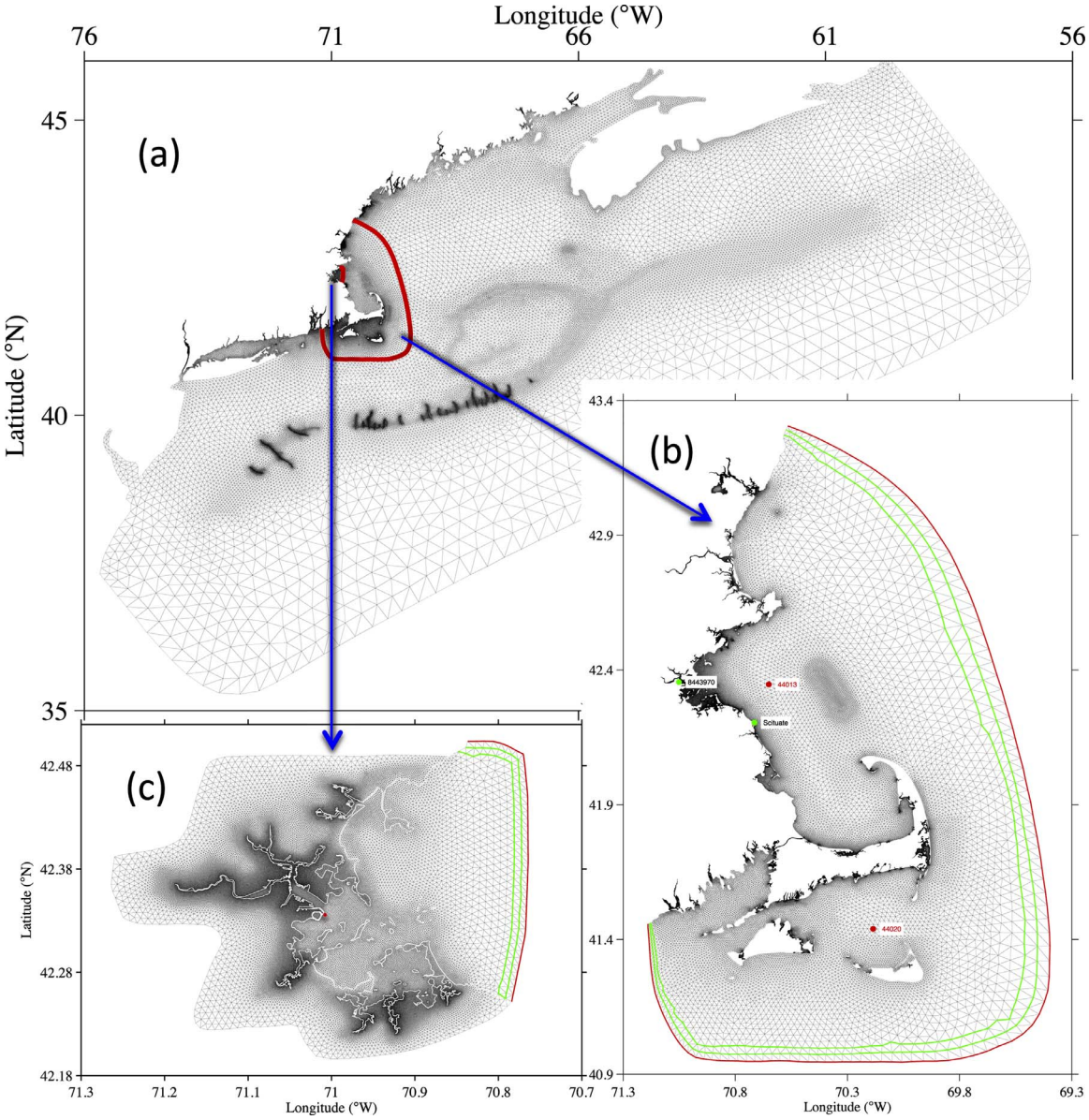

Fig. 4. The grids of the regional GOM-FVCOM domain (a), MASS Coastal-FVCOM domain (b) and MASS Bay-FVCOM domain (c) used to establish two-domain nested models in Sections 3 and 4, respectively.

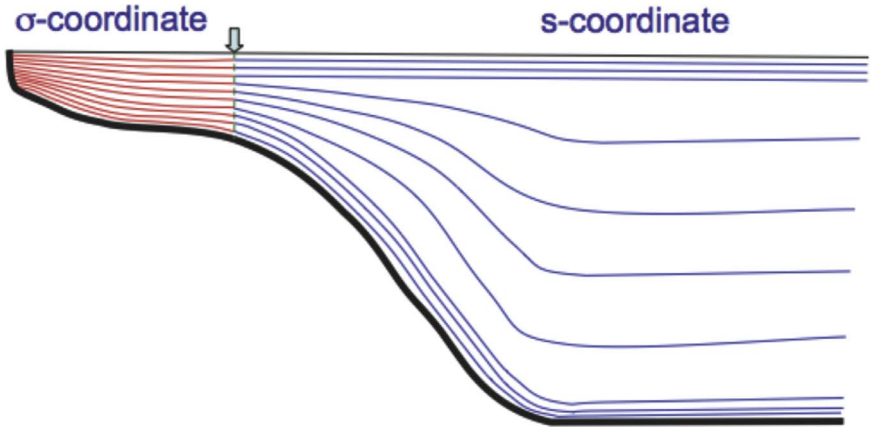

Fig. 5. An illustration of a hybrid coordinate consisting of σ- and *s*–coordinates (from Chen et al., 2013a).

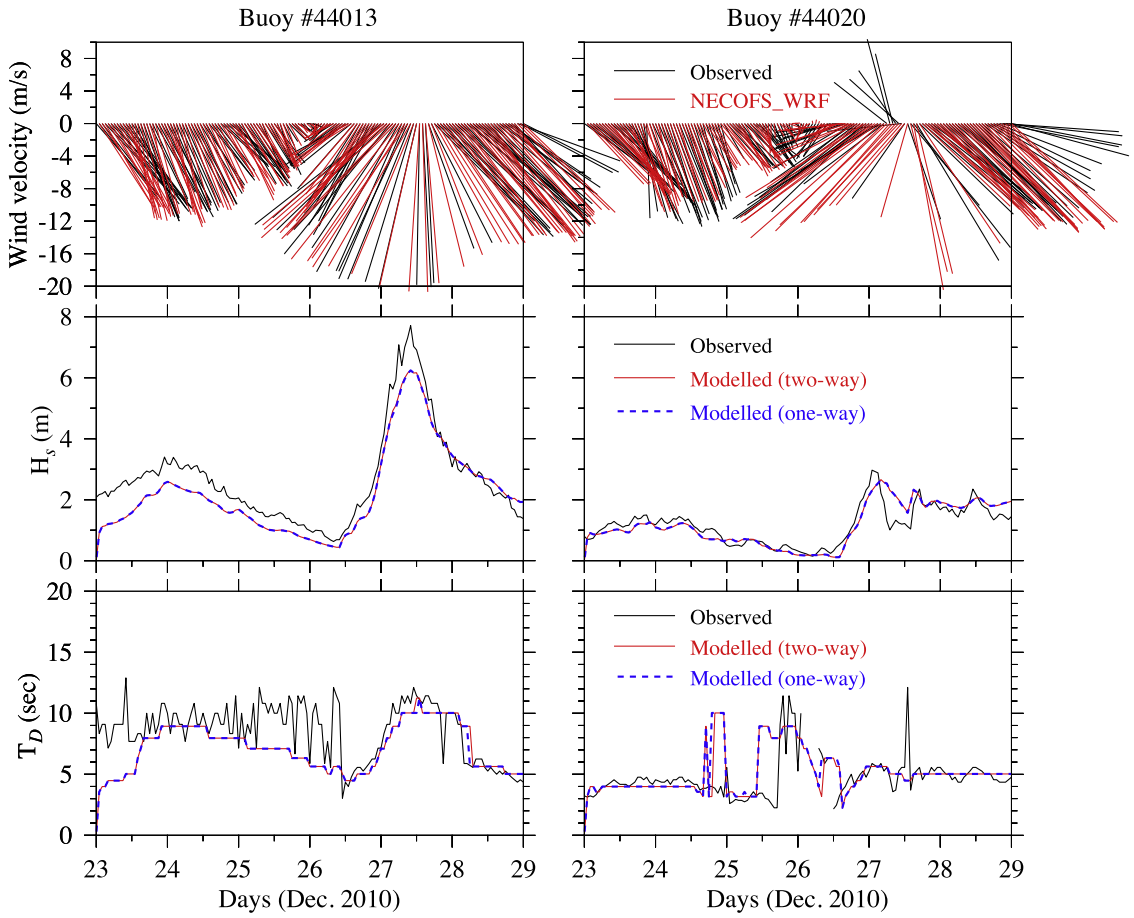

Fig. 6. Comparisons of the observed and model-simulated wind vectors, significant wave heights and peak periods at buoys #44013 (inside the Mass Bay) and #44020 (in the Nantucket Sound). The wind simulation was done by NECOFS-WRF, and the model-simulated surface waves were done by the nested model with one-way and two-way nesting approaches, respectively.

processors separately via the ESMF. The data exchanges between the large and small domain nesting boundaries are carried out using the entire number of processors that the nesting system uses.

This nesting system was originally developed for the two-way nesting, but it can be used for a simpler one-way nesting case when turning off the "Run CplComp (S->L)" controller in the do-loop of the second column shown in Fig. 2.

The procedures of time integration and nesting data exchange between large and small domains are illustrated in Fig. 3a. The red lines indicate the data from large domain to small domain, while the green lines represent the data feedback from small domain to large domain. The frequency of the data exchange between two domains is based on the time step of large domain. Let us define Δt_l and Δt_s as the time steps used for large and small domains, respectively. $\Delta t_l = n\Delta t_s$, where n is an integer. First, when the large domain is integrated over one time step Δt_l from the time t to the time $(t + \Delta t_l)$, the nesting data in the large domain are sent to the small domain as the open boundary condition of the small domain. Then, when the small domain is integrated for n time steps of Δt_s to the time of $t + \Delta t_l$, the data in the small domain are feedback to the large domain.

The data exchange between large and small domains is illustrated by a sketch map in Fig. 3b. The red line was defined as the nesting boundary of the small domain on which the variables at nodes and cells (connected to this red line) were provided by variables computed at the same nodes and cells in the large domain. The area between the two green lines was where the simulated variables in the small domain gave feedback to the same nodes and cells in the large domain.

3. A wave-current interaction experiment

3.1. The experiment designs

The Northeast Coastal Ocean Forecast System (NECOFS), as one component of the NOAA IOOS-funded Northeastern Regional Association of Coastal and Ocean Observing Systems (NERACOOS), is an integrated atmosphere/surface wave/ocean forecast model system designed for the northeast U.S. coastal region, covering a computational domain from the Delaware Shelf to the eastern end of the Scotian Shelf, including the New England Shelf (NES), Georges Bank (GB) and the Gulf of Maine (GOM) (Fig. 4a). NECOFS was placed in experimental forecast operations in late 2007. The present system includes 1) a community mesoscale meteorological model named "Weather Research and Forecasting (WRF)"; 2) the regional FVCOM with the computational domain covering the Gulf of Maine/Georges Bank/New England Shelf region (GoM-FVCOM); 3) the unstructured-grid surface wave model (GoM-SWAVE) modified from SWAN (Qi et al., 2009) with the same domain as GoM-FVCOM; 4) the Mass Coastal FVCOM with the inclusion of estuaries, inlets, harbors and intertidal wetlands; and 5) 4 subdomain wave-current coupled FVCOM inundation forecast systems in Scituate Harbor, MA; Boston Harbor, MA; Hampton-Seabrook Estuary, NH and Saco Bay, ME.

The GoM-FVCOM grid features unstructured triangular meshes with horizontal resolution of ~ 0.3–25 km (Fig. 4a) and a hybrid terrain-following vertical coordinate (with a total of 45 layers, 10 and 5 uniform layers near the surface and bottom, respectively, in regions deeper than 225 m with a transfer to a sigma-coordinate in the shallow continental and coastal regions). An example of the distribution of the

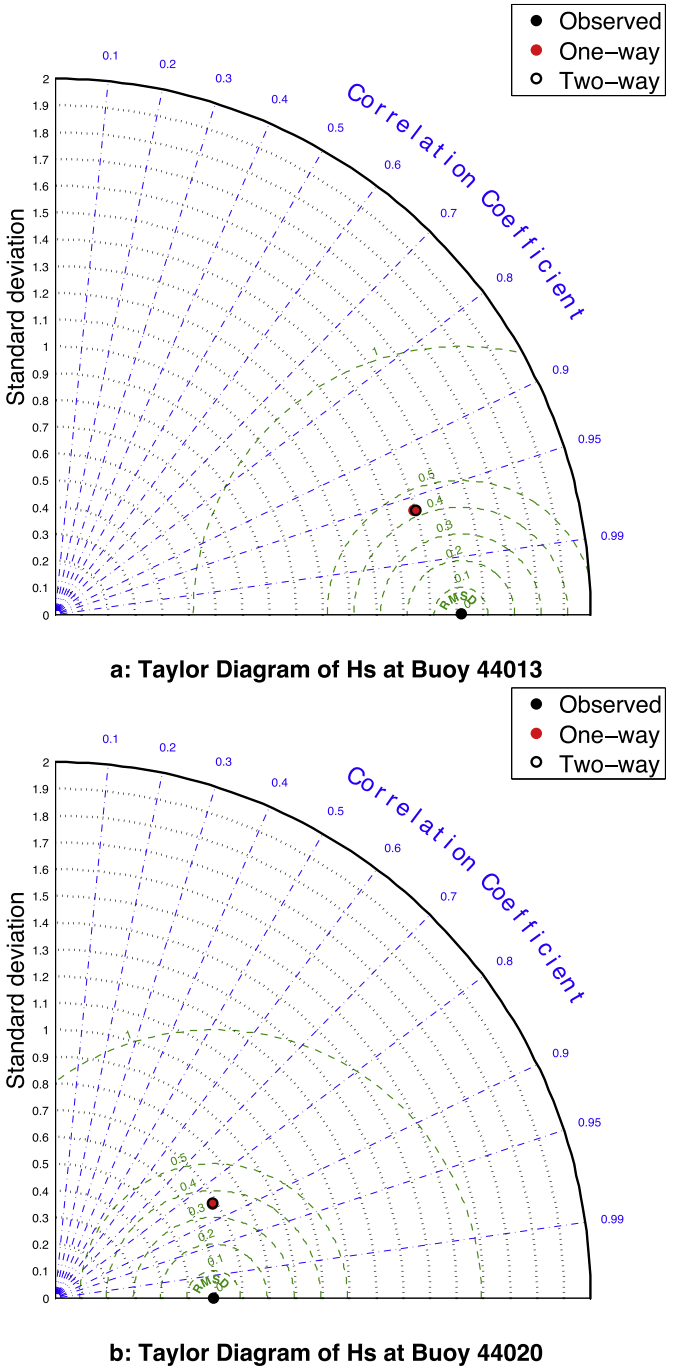

Fig. 7. Taylor diagrams showing RMSD and correlation coefficients for the model-data comparison of the significant wave height at buoys #44013 (a) and #44020 (b).

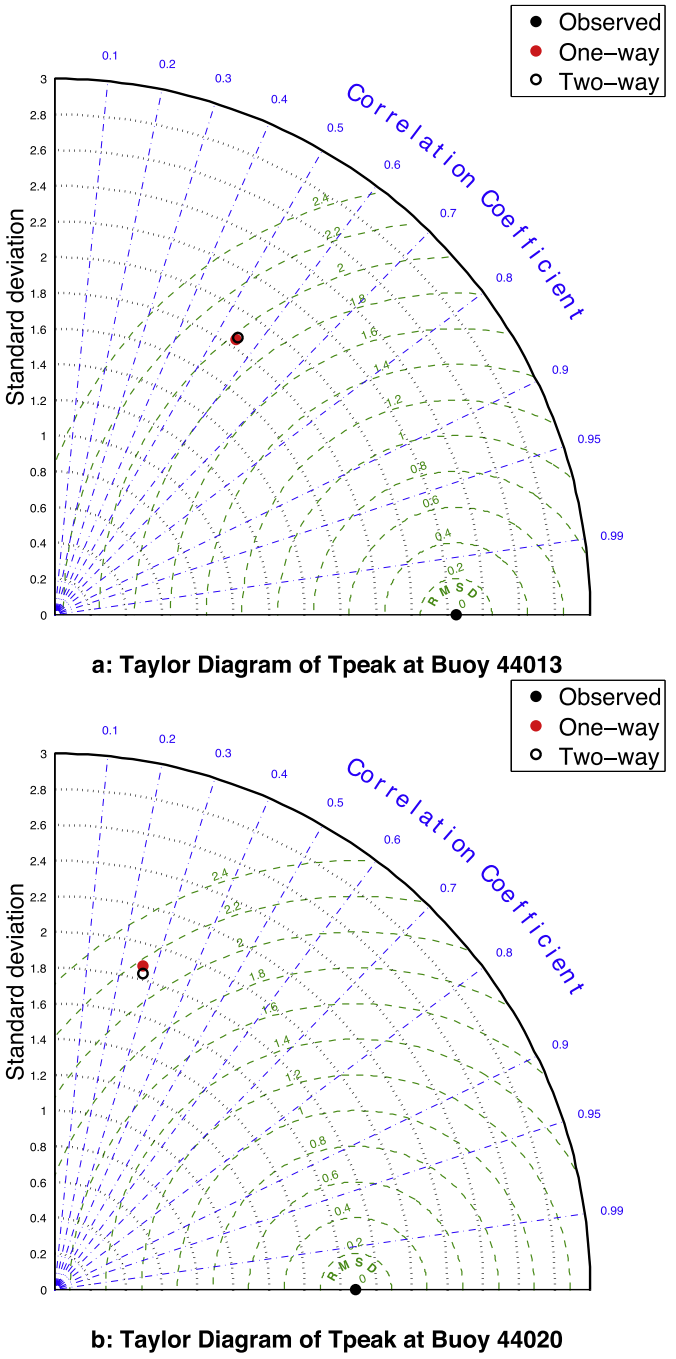

Fig. 8. Taylor diagrams showing RMSD and correlation coefficients for the model-data comparison of the peak wave period at buoys #44013 (a) and #44020 (b).

vertical layers in the hybrid coordinate is displayed in Fig. 5. The thickness of the uniform layers is 5 m, so the hybrid coordinate transition occurs at locations where all layers have uniform thickness of 5 m. The Mass Coastal-FVCOM grid is configured with triangular meshes with horizontal resolution up to ~ 10 m (Fig. 4b), and 10 layers in the vertical. Four inundation model grids include both the water and land with horizontal resolution up to ~ 5–10 m and 10 vertical layers.

GoM-FVCOM is driven by surface forcing from the output of the WRF model configured for the region (with a 9-km resolution), the COARE3 bulk air-sea flux algorithms, tidal forcing constructed using five constituents (M_2, S_2, N_2, K_1 and O_1) on the open boundary, and local river discharges. The GoM-SWAVE is driven by the same WRF wind field with wave forcing at the boundary nested to Wave Watch III (WWIII). WWIII is set up for a northwestern Atlantic region and run at the same time when the WRF forecast is carried out. The Mass Coastal-FVCOM and four inundation models are connected with GoM-FVCOM through the offline "one-way" nesting in the common boundary zones. The Mass Coastal-FVCOM is driven by the same surface forcing as GoM-FVCOM. The nesting boundary conditions for the inundation models include both hydrodynamics and waves provided by GoM-FVCOM and GoM-SWAVE. NECOFS was placed in experimental forecast operations in late 2007 and the daily 3-day forecast product can be accessed and viewed on the NECOFS Web Map Server addressed: (http://134.88.229.220:8080/fvcomwms/).

An experiment was made on running the GoM-FVCOM and Mass Coastal-FVCOM nested ocean model system in NECOFS simultaneously using the one-way and two-way nesting approaches on the ESMF

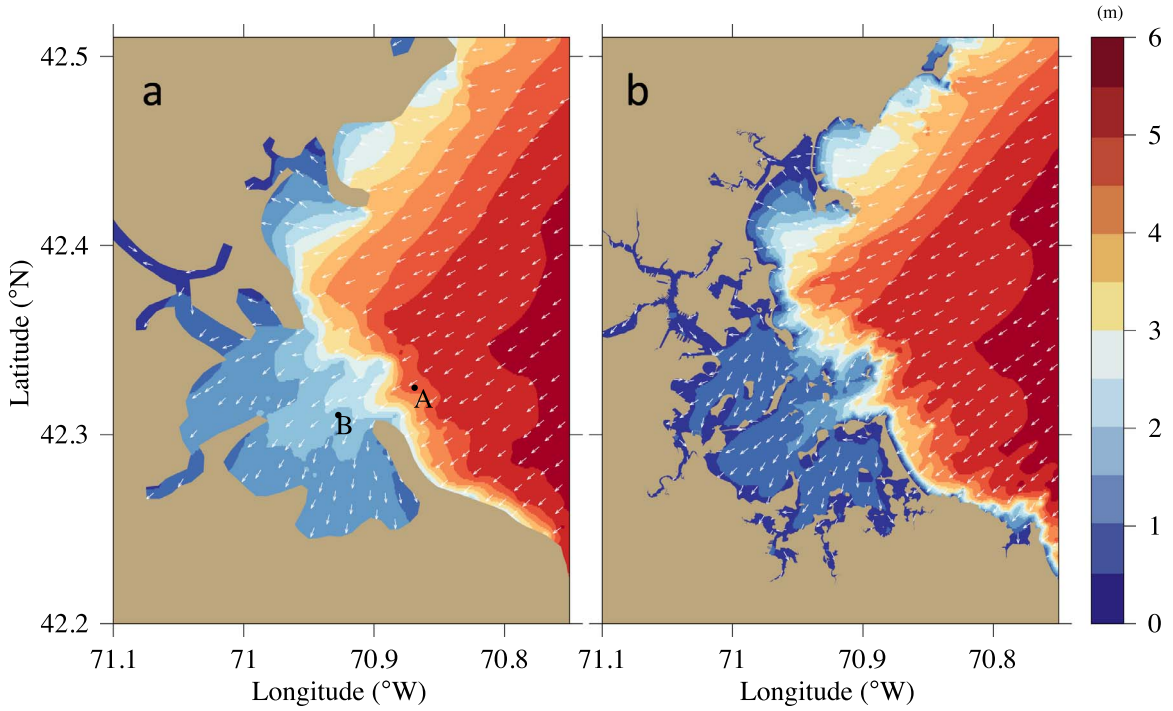

Fig. 9. Comparisons of the distributions of surface wave heights and directions in the Boston Harbor area at 11:00 UTC on December 27, 2010 for (a) large- and (b) small-domain models.

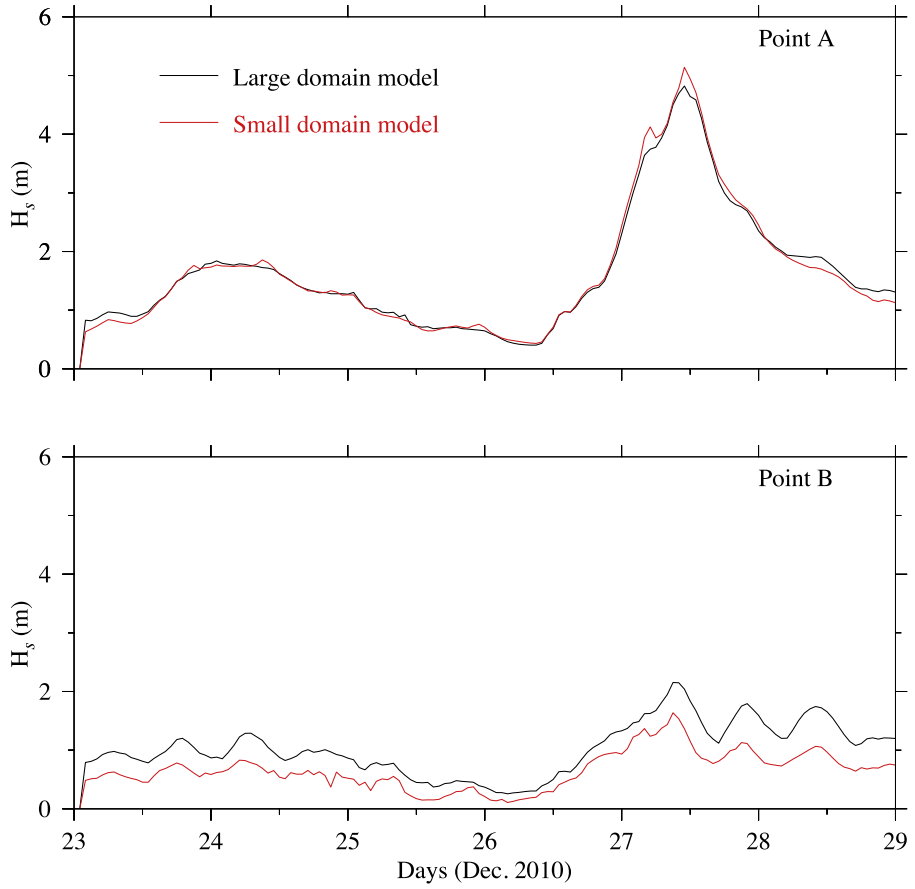

Fig. 10. Time series comparisons of the significant wave heights at sites A (upper) and B (lower) produced by the large-domain and small-domain models. Locations of sites A and B shown in Fig. 9a.

coupler. In this case, the large domain referred to the GoM-FVCOM domain (Fig. 4a) and the small domain referred to the Mass Coastal-FVCOM domain (Fig. 4b). In the large domain, the area enclosed with the red line was the small domain. In the small domain, the meshes enclosed within the red and green lines shared the same elements with the large domain. Time integration and nesting data exchange between

Table 1
The mean, averaged differences, maximum and maximum difference values of significant wave heights at site-A and site-B shown in Fig. 9 for the model-data comparisons made using the large and nested small-large domain model runs.

Point	Mean (m) (large)	Mean (m) (small)	Mean difference (m)	Max (m) (large)	Max (m) (small)	Max difference (m)
A	1.630	1.627	0.003	4.821	5.140	0.319
B	1.023	0.657	0.367	2.153	1.637	0.716

Mass Coastal-FVCOM and GoM-FVCOM follow the procedures described in Section 2.

The model-data comparisons were made at available observations in the small domain. There were two buoys (red dots in Fig. 4b) and two tidal gauges (green dots in Fig. 4b) in the Mass Coastal-FVCOM domain. Buoy #44013 was located in Mass Bay and buoy #44020 was in Nantucket Sound (http://www.ndbc.noaa.gov). On these buoys, the wind velocity and significant wave heights/frequency were measured, and hourly records were made in the comparison. One tidal gauge named #8443970 was within the Boston Harbor (https://tidesandcurrents.noaa.gov) and another was in the Scituate Harbor, MA. These two areas were not resolved in the large domain. The tidal gauge in the Scituate Harbor was deployed by R. Thompson (NWS Taunton WFO) and F. Peri (UMass-Boston) in December 2008 (Chen et al., 2013b).

The nested model ran with the inclusion of wave-current interaction by one-way and two-way nesting, respectively. The simulation was conducted for the December 27, 2010 Nor'easter storm, with the integration time covering the period of December 23–29. The initial conditions used in the two domains were given from the NECOFS hindcast database. The December 27 Nor'easter storm was one of largest storms that had swept over this Mass coastal region, with a maximum wind speed of >20 m/s (Beardsley et al., 2013).

3.2. Waves comparisons

During the simulation period, the northerly wind prevailed. In Mass Bay, the strongest wind occurred around 11:00 UCT December 27, 2010, at which the northeasterly wind was dominate and its speed recorded on buoy #44013 exceeded 20 m/s. The maximum significant wave height occurred at the same time as the maximum wind speed, with its highest value of 7.7 m and a peak period of ~ 10 sec. NECOFS-WRF was capable of reproducing the wind velocity at this station. Under the same wind forcing condition, the model-predicted significant wave heights and peak periods from the one-way and two-way nesting approaches were almost identical (Fig. 6: left panel), with the root-mean-square deviations (RMSD) of 0.42 m and 1.94 s, respectively. The Taylor diagrams of RMSD and correlation coefficient are shown in Fig. 7a for significant wave height and in Fig. 8a for peak wave periods. We also ran the model with a single mesh by merging the small domain grid with the large domain, with the results remaining the same but much more computational cost. This suggested that the model-data difference appeared in the figure was not related to either one-way or two-way nesting methods used in the experiment. This comparison result indicated that the nesting method coded under the ESMF framework performed well. In this case, the one-way nesting was sufficient, and no two-way nesting was needed. This finding was not surprising, since the storm-induced surface waves observed at this station mainly consisted of wind-sea and swells. The wind-sea was generated by the local wind, while swells were the waves propagated from the outer shelf of Mass Bay.

Similar results were found on buoy #44020 in Nantucket Sound (Fig. 6: right panel). Nantucket Sound is bounded by Cape Cod on the north, Martha's Vineyard on the southwest and Nantucket Island on the southeast. The storm-induced surface waves were much weaker in Nantucket Sound than those observed in Mass Bay, even though the wind intensification was similar in these two regions. The maximum significant wave height at buoy #44020 was about 3.0 m, occurring around 00:00 UCT, December 27. The model reasonably captured the significant wave height and peak period. As found at buoy #44013, the model-predicted significant wave heights and peak periods were almost identical in both one-way and two-way nesting cases (Figs. 7b and 8b).

The offline one-way nesting used in NECOFS was operated using the same cluster nodes for both large and small domains, and they were required to run one after another. The one-way nesting coupler on the ESMF framework allowed the two domains to run simultaneously, which could help maximize the use of the supercomputer nodes.

The two-domain nesting approach enables one to increase the

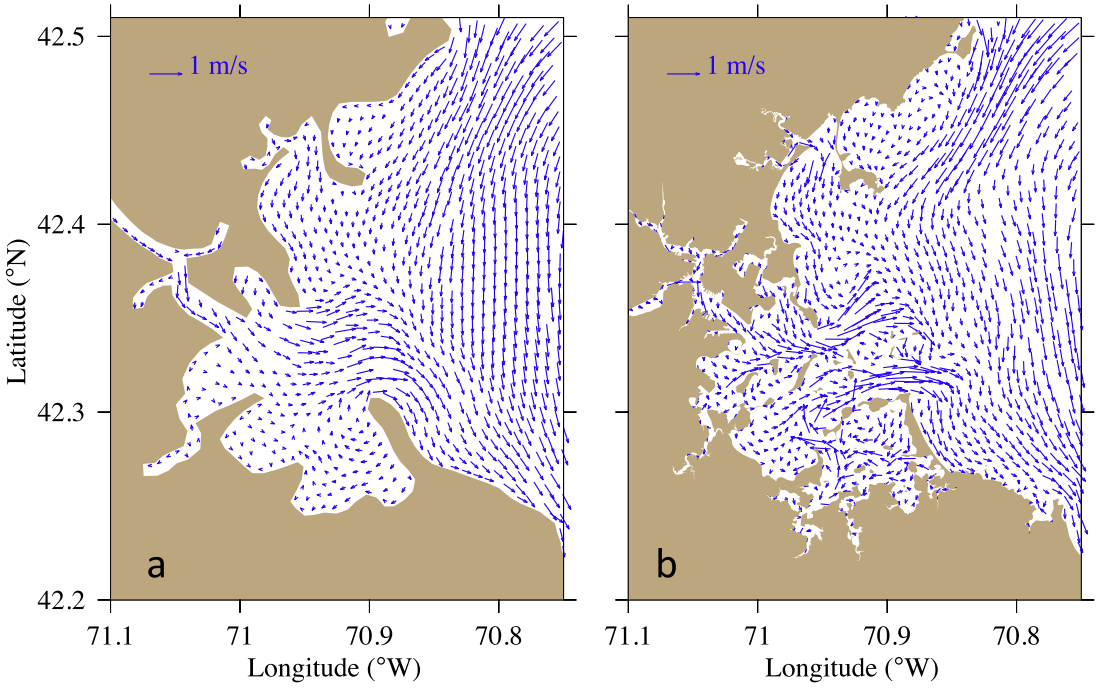

Fig. 11. Comparisons of the distributions of surface current vectors in the Boston Harbor area at 11:00 UTC on December 27, 2010 for (a) large- and (b) small-domain models.

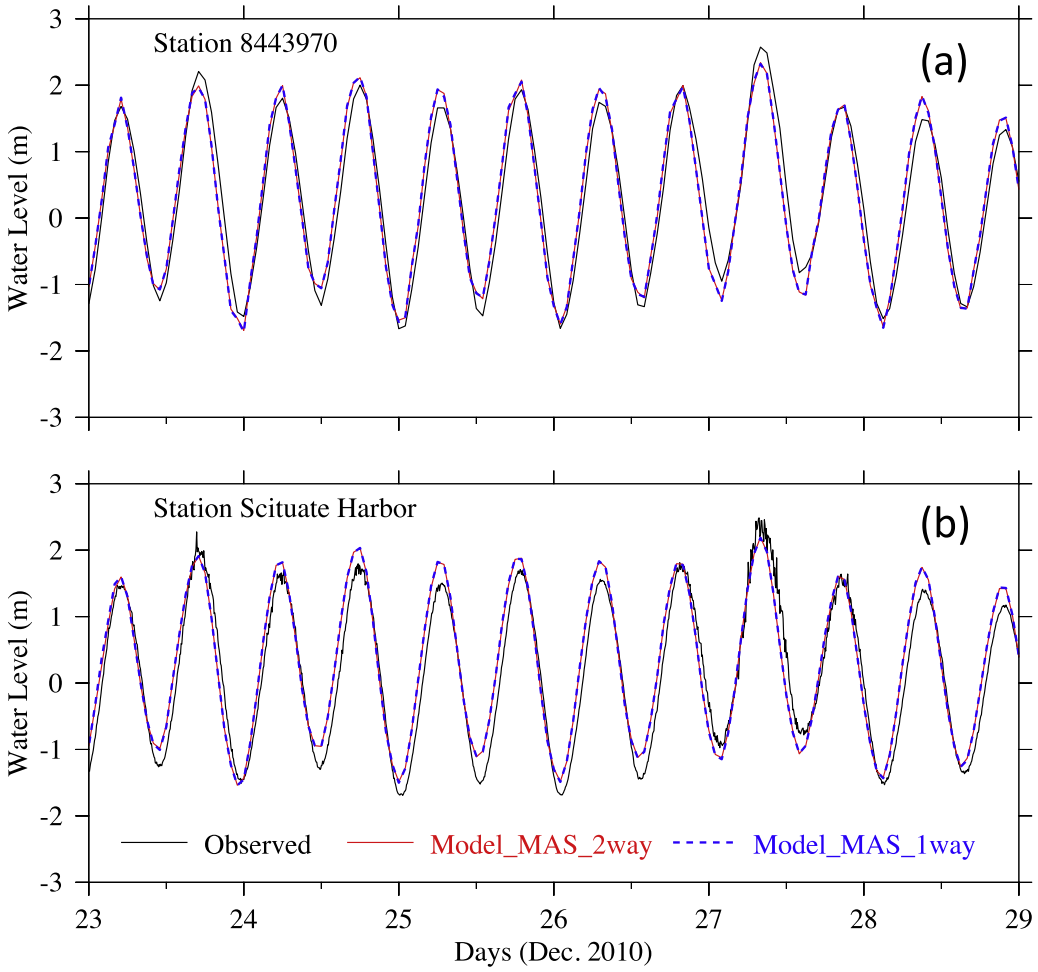

Fig. 12. The time series comparison of observed and model-simulated water elevations at the Boston Harbor tide station 8443970 (a) and the Scituate Harbor tide station (b). The black lines: Observed; the red lines: two-way nesting and the dashed blue lines: one-way nesting. (For interpretation of the references to color in this figure legend, the reader is referred to the web version of this article.)

model grid spatial resolution near the coastal region with no significant sacrifice in computational efficiency, particularly in the areas characterized with narrow water passages, islands, inlets and rivers. An example is illustrated in Fig. 9, where snapshots of the distributions of the significant wave heights plus propagation directions in the Mass Bay/Boston Harbor show the large (Fig. 9a) and small (Fig. 9b) domain model results. The large domain model had a horizontal resolution of ~300 m in the Boston Harbor area, which failed to resolve numerous islands and complex irregular coastline in that area. The small domain model had a horizontal resolution of ~10 m, which was sufficient to accurately capture those islands and irregular coastline. Due to the lack of the blocking mechanism by those solid obstacles, the large-domain model tended to produce a higher wave height in the harbor area. The difference can be viewed more clearly at sites A outside of the harbor and B inside the harbor illustrated in Fig. 10 and Table 1. The locations of sites A and B were shown in Fig. 9a. The storm-induced waves propagated towards the coast from the outer Mass Bay shelf. At point A, the wave heights predicted by the large-domain and small-domain models were close each other, except at the time when the waves were highest. At that time, the simulated maximum wave was about 0.32 m higher in the small-domain model than in the large-domain model. At point B, however, the simulated waves produced by the large-domain model were generally about 0.37 m higher, with a maximum difference up to 0.72 m. This comparison clearly demonstrated a need to increase the model resolution in the coastal wave simulation and such a requisite can be efficiently achieved by a nested domain model approach.

3.3. Current and sea level comparisons

The nesting approach also helped a model to resolve the complex spatial distribution of the currents inside Boston Harbor. An example is shown in Fig. 11 for the comparison of the surface currents in the harbor area at 11:00 UCT, Dec. 27, 2010. At that time, currents outside of the harbor were dominated by the wind-induced inflow, but the water inside the harbor was flushed out. In the large-domain model (Fig. 11a), due to missing of islands inside the harbor, the outflow was relative-uniformly distributed. Nesting allowed the small domain model to include all islands inside the harbor. As a result, the outflow featured two strong current jets through the islands (Fig. 11b), although the total outflow transports obtained from large and small domain models were close to each other. It is clear that the nesting model provided a more realistic flow pattern in the harbor area, which is critically important for capturing the spatial distribution of the storm-induced coastal inundation.

We also compared the observed water elevation with model-simulated elevations predicted by the one-way and two-way nesting approaches at the Boston Harbor tidal gauge station #8443970 and the tide station in Scituate Harbor (Fig. 12). Note here that these two stations were not resolved in the large-domain model. It was not surprising that no significant difference was found in the model-simulated elevations predicted by the one-way and two-way nesting approaches (Fig. 13), since these two stations were located inside harbors, which was far away from the nesting boundary. Tidal currents are periodic motions that were not affected by nesting if the tidal elevation is

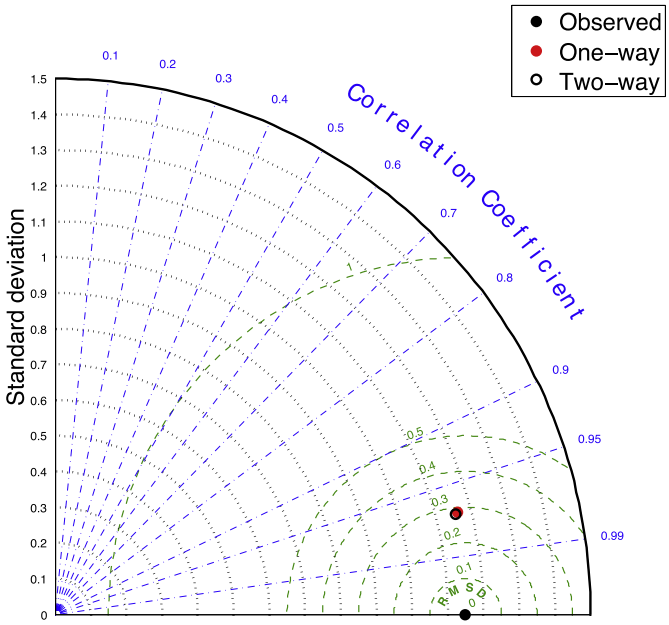

a: Taylor Diagram of Elevation at Station 8443970

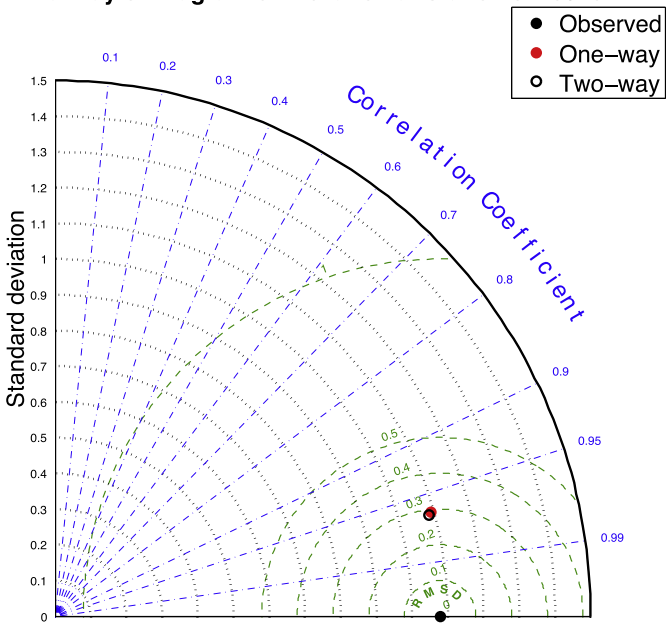

b: Taylor Diagram of Elevation at Station Scituate Harbor

Fig. 13. Taylor diagrams showing RMSD and correlation coefficients for the model-data comparison of the water elevation at stations 8443970 (a) and Scituate Harbor (b).

accurately given at the nesting boundary. During the simulation period, the onshore northeasterly wind prevailed, with interacting with surface waves, the wind pushed the water towards the coast. On the nesting boundary, the tidal currents were the same for both small and large domains and the wind-induced subtidal flow was onshore, so that no significant feedback flow from the small domain to large domain appeared.

4. Salinity plume simulation experiments

The current-wave interaction experiment described in Section 3 was done under a Nor'easter storm during which the inflow was dominant. In that case, we found that the one-way and two-way nesting showed no significant differences in the results for the high-resolution small domain model. Here we present the salinity plume case with the flow towards the nesting boundary from the small domain to the large domain, illustrating the importance in having two-way nesting. Two experiments were made for the salinity plume. First, we conducted the plume case with a point source over an idealized rectangular continental shelf with a constant depth and then a point source case in Boston Harbor configured with the nested Mass Bay FVCOM and GoM FVCOM system.

4.1. An idealized continental shelf

The experiment was made over a constant-depth idealized rectangular continental shelf with a length of 30 km and a width of 5 km. To view the grid in the domain clearly, the portion of the left 10-km computational domain are shown in Fig. 14a and d. Experiments were made for the cases with 1) a single merged domain (named "the standard run") solved without nesting, 2) two domain solved through the one-way nesting, and 3) two domains solved through the two-way nesting. We assumed that the results from 1) are the "true solution", and the model performance for one-way and two-way nesting methods are evaluated through the comparison with the "true solution" obtained from the standard run.

The large-domain model was configured with a resolution of 250 m in the almost whole domain except near the point source area, where a resolution of 125 m was specified (Fig. 14a). The small-domain models were configured with a resolution of 125 m everywhere except in the overlapping meshes zone connected to the nesting boundary with the large-domain model (Fig. 14b and c). For the two-way nesting experiments, to examine the sensitivity of the model performance to the location of the nesting boundary, we ran the model for two cases with different locations of the nesting boundary of the small domain to the large domain, and named the cases "Case-a" and "Case-b". In Case-a (Fig. 14b), there were only two layers of overlapping cells beside the nesting boundary from the large domain to the small domain. The nesting boundary from the small domain to the large domain is located at the second layer of overlapping cells. In Case-b (Fig. 14c), there were five layers of overlapping cells. The nesting boundary from the small domain to the large domain is located at the fifth layer of overlapping cells. A single merged domain was constructed by the small domain in Case-a with the rest region filled using the large domain grid (Fig. 14d). In Fig. 14, the red dot in each figure was the location where the point source was specified. The one-way nesting experiment was run with the configuration of two domains like Case-a, except that the feedback from the small domain to the large domain was turned off. In all experiments, both large-domain and small-domain models used uniform-thickness layers with a total of 11 levels in the vertical. The radiation boundary conditions were employed at the large domain open boundary.

Initially, a constant salinity of 30 PSU was specified everywhere. Water with a salinity of 10 PSU was discharged into the domain at a constant rate of 100 m^3/s from the point source. The nested model was integrated for 9 days.

The snapshots of the spatial distribution of model-simulated surface salinity, which were predicted from the standard run with a single merged grid without nesting at the end of 3 and 9 days were shown in Fig. 15a and e, respectively. Taking the standard run results as "true solution", an assessment was done for one-way and two-way nesting methods through comparing their results with the "true solution". The comparison results clearly showed that the simulated surface salinity through the one-way nesting led to a significant bias around the nesting boundary and in the large domain region (Fig. 15b and f). Sites-A and B in Fig. 15b and f were the locations where the maximum errors appeared at the nesting boundary at the end of 3 and 9 days, respectively. At these two sites, the simulated salinity started deviating from the true solution after the 12-hour simulation time and maximum deviation reached 0.29 at site-A and 0.21 at site-B after 9-day simulation time (Fig. 16). The error reduced significantly when the two-way nesting was

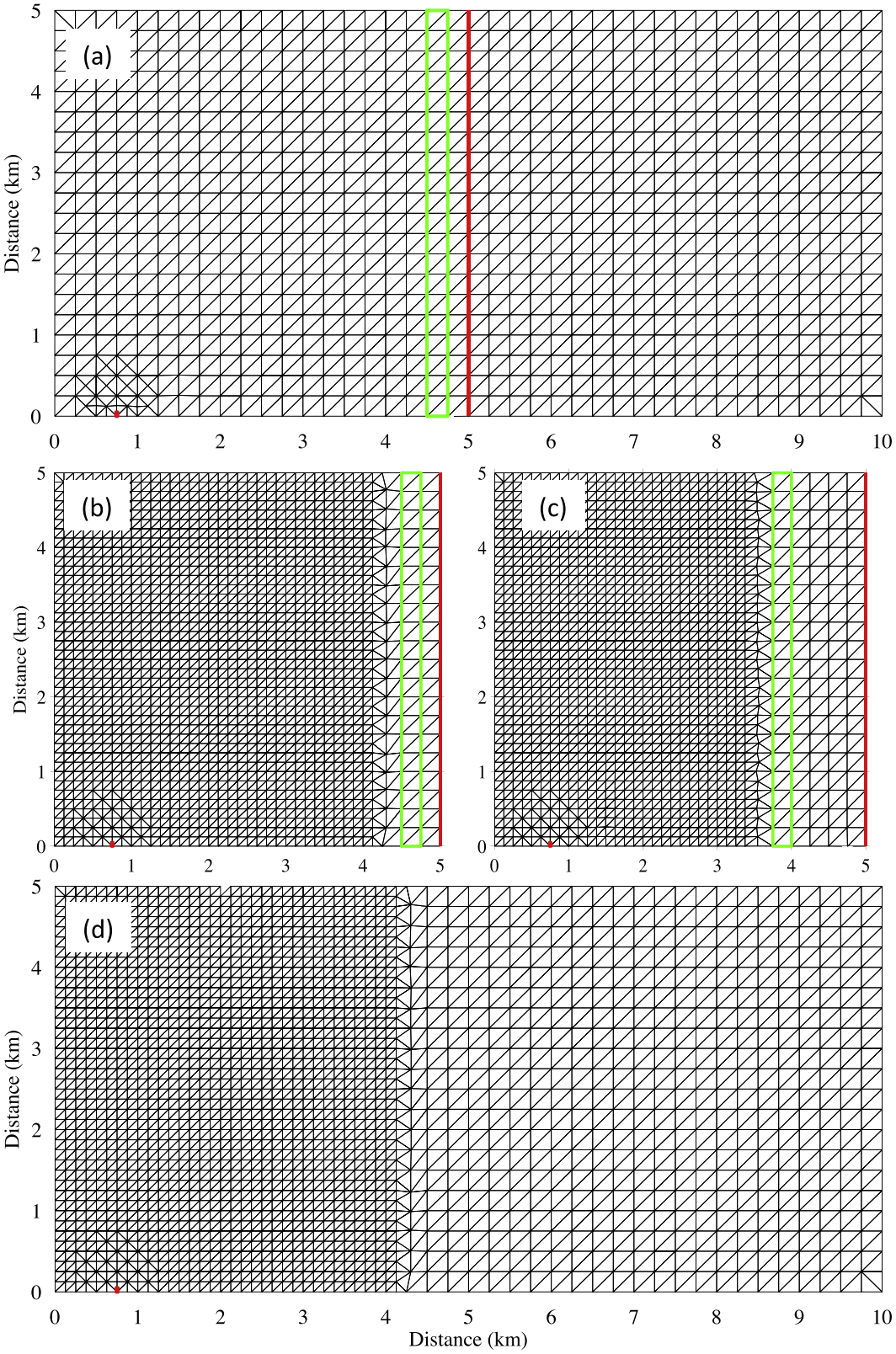

Fig. 14. The large and small domain grids configured for the idealized, constant-depth continental shelf cases. (a): large domain (note: only the left 10-km region was shown); (b): the small domain for Case-a; (c): the small domain for Case-b; (d): a single merged domain constructed using the nested domain used for Case-a (note: only the left 10-km region was shown). The definitions of red and green lines were given in the text. (For interpretation of the references to color in this figure legend, the reader is referred to the web version of this article.)

turned on. In both Case-a and Case-b, the simulated surface salinity exhibited the almost same distribution and values in the entire computational domain, including at the nesting boundary (Fig. 15c, g for Case-a and Fig. 15d, h for Case-b). At site-A and site-B, the maximum deviation errors were 0.02 in Case-a and 0.06 in Case-b, showing the error reduction of 93% and 79% respectively, compared with the one-way nesting case (Fig. 16). A statistical analysis of the errors was presented through the Taylor diagram shown in Fig. 17, where the RMSD

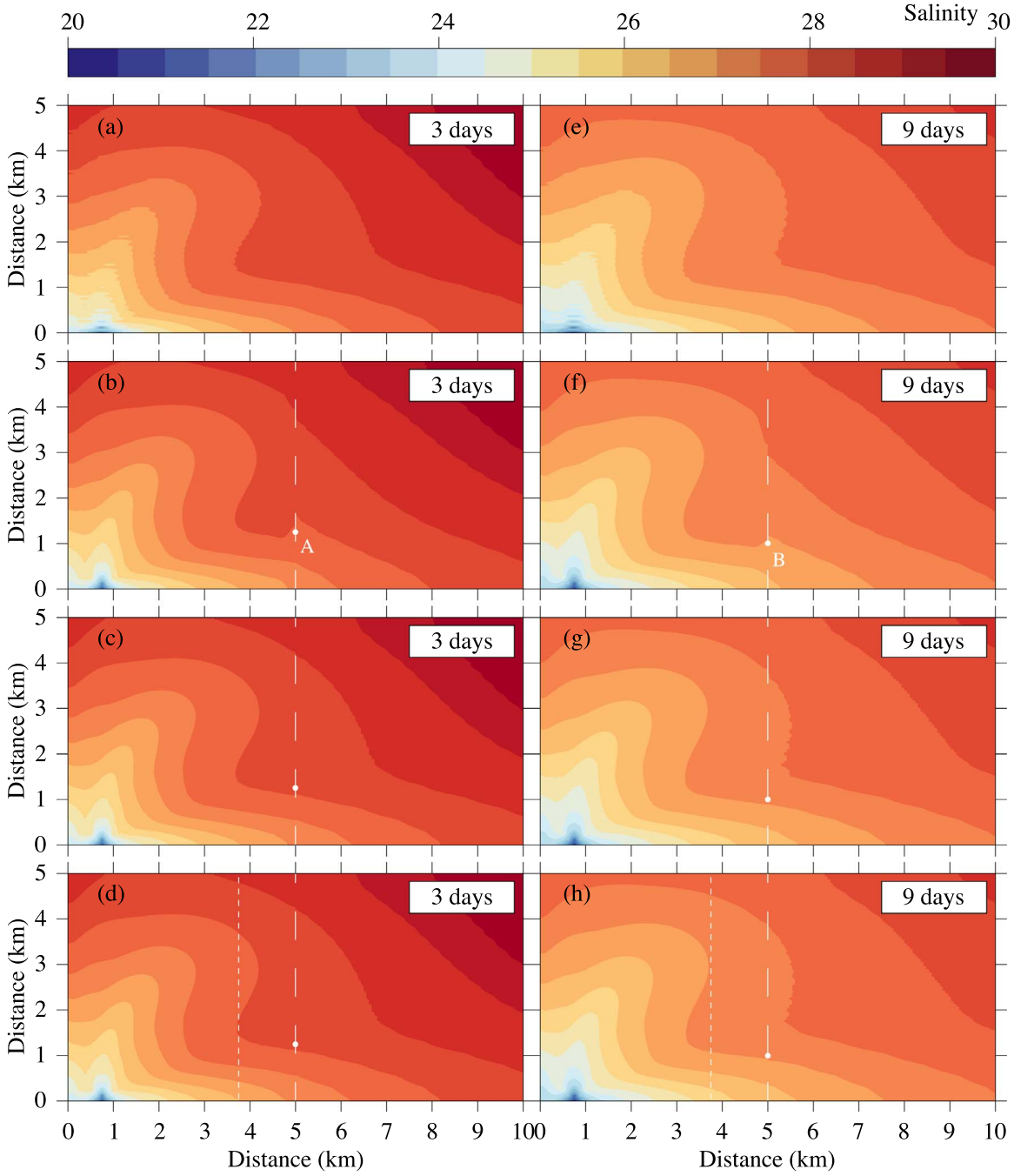

Fig. 15. Comparisons of the distributions of the model-simulated salinity plume in the computational domain produced by a single merged-domain model run without nesting (a and e), the one-way nested model run (b and f), two-way nested model for Case-a (c and g) and two-way nested model run for Case-b (d and h) at the end of 3 day (left panels) and 9 day (right panels). For the nested model cases, the salinity was drawn by merging the large- and small-domain model results.

and correlation coefficients of the comparison results of the one-way and two-way nesting model runs with the single merged domain standard model run were presented.

It is clear that in the one-way nesting case, the water in the small domain was blocked when it entered the nesting zone. With grid refinement in the small domain, the model-simulated structure of the low-salinity plume in the small domain significantly differed from that produced by the large domain model. In the one-way nesting case, as the integration time becomes longer, when the plume's edge reached the nesting boundary, the velocity, sea level, and salinity produced by the small-domain model differed from the boundary conditions provided by the large-domain model. As a result, the water was blocked near the nesting boundary, which clearly appeared in the distribution of the salinity by merging the large- and small-domain model results (Fig. 15b and f). This block disappeared when the two-way nesting was used (Fig. 15c and g). The two-way nesting not only included a feedback boundary condition from the small-domain model to the large-domain model but also adjusted the boundary forcing to the small domain. The two-way nesting method developed in the FVCOM on the ESMF framework performed well to avoid the mass accumulation at the nesting boundary. This example illustrates the need for having a two-way nesting in addition to demonstrating how well this method performed.

The comparison results for Case-a and Case-b clearly show that the location of the nesting boundary from the small domain to the large domain affects less to the distribution of the salinity. The simple merged

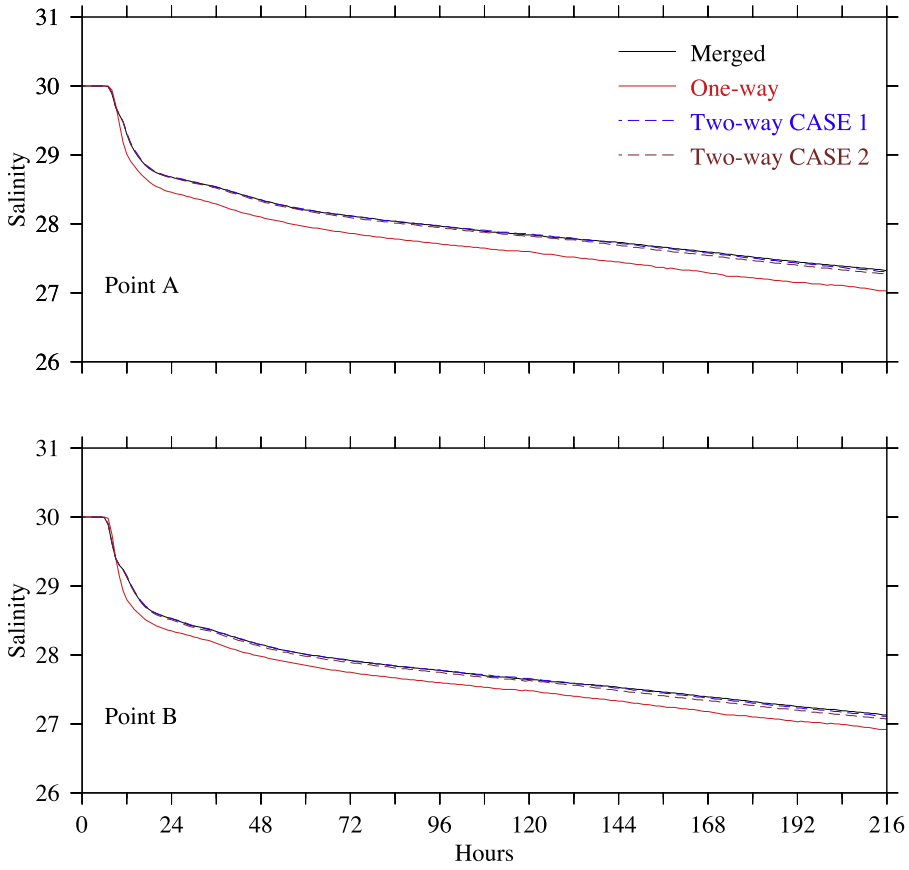

Fig. 16. The comparison of the time series of the model-simulated salinity at site-A and site-B (shown in Fig. 15) for the one-way and two-way nesting cases.

domain case (Fig. 14d) for 'true resolution' was designed based on Case-a. The comparison between this 'true resolution' and Case-b is not reasonable. This comparison only illustrated that the configuration for Case-a is simple and efficient with enough accuracy.

4.2. A realistic geometric case in Boston Harbor

NECOFS has setup a FVCOM inundation model for Mass Bay (named Mass Bay-FVCOM) with the small domain grid shown in Fig. 4c. This small-domain model is being operated by one-way nesting with the regional GOM-FVCOM in NECOFS. We used this nested model to repeat the point source experiments conducted in Section 4.1 to see how the one-way and two-way nesting methods in the FVCOM performed in a realistic geometric domain case. The FVCOM inundation model for Mass Bay (hereafter referred to as the small domain model) was configured with a horizontal resolution varying from 10 m to 500 m and a total of 11 uniform-thickness sigma levels in the vertical. The red and green lines shown in Fig. 4c had the same definitions as those shown in Fig. 3b.

The nested model was run by injecting low-salinity water as a point source at the location marked with a red dot in Fig. 4c for the one-way and two-way nesting approaches, respectively. A constant salinity of 30 PSU was specified everywhere initially, then low-salinity water with a constant salinity of 10 PSU was injected at a rate of 2000 m^3/s into the domain from the point source. The simulation was conducted for a period of 3 days. The tide was included in this case.

As was found in the idealized rectangular continental shelf case, the one-way nesting approach caused the low-salinity plume water to be blocked when it entered the nesting boundary zone (Fig. 18b). Mismatching of the salinity between small- and large-domain models rapidly increased as the integration time became larger. This error disappeared when two-way nesting was applied.

Grid refinement in the small-domain model captured complex islands in Boston Harbor, which produced significant spatial variability of the low-salinity plume in the small-domain. The spatial distribution and intensity of the flow and salinity plume produced by the small-domain model considerably differed from those in the large-domain model (Fig. 18a). The mismatch of velocity and salinity between large- and small-domain models in the nesting boundary zone caused the blocking phenomenon and a gap of the salinity in that region (Fig. 18b). There was no question that in such a case, the two-way nesting was required (Fig. 18c).

Selecting the transect indicated in Fig. 18a, we plotted the vertical distribution of the salinity for the case runs with a single large domain and nested small-large domain (Fig. 19). In the nested small-large domain model runs, we included the results for the one-way (Fig. 19b) and two-way (Fig. 19c) experiments. As we described above, the simulated salinity from the single large domain model run was not comparable with the nested small domain model runs since it failed to resolve the detailed geometry in the inshore area of the harbor (Fig. 19b). Comparing the salinity distribution shown in Fig. 19b for one-way nesting and in Fig. 19c for two-way nesting, we did see that in the one-way nesting case, blocking at the nesting boundary tended to produce a large along-transect salinity gradient inside the small domain. The two-way nesting case accounted for the feedback from the small domain to the large domain. As a result, the salinity plume was carried out of the small domain, producing an enhanced halocline in the large domain region. In turn, the horizontal salinity gradient in the small domain reduced.

5. Summary and discussion

The FVCOM was implemented into the ESMF framework to set up the one-way and two-way nesting modules for the unstructured-grid

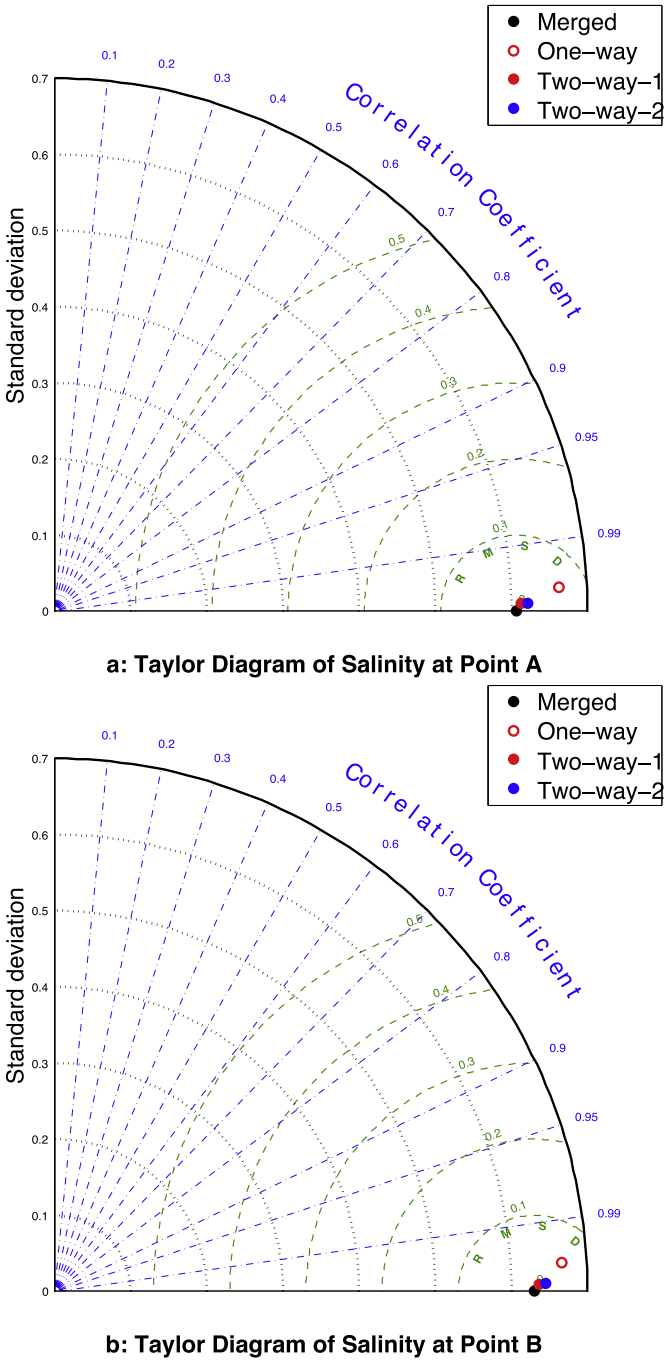

Fig. 17. Taylor diagram showing RMSD and correlation coefficients for the salinity comparison at site-A and site-B (shown in Fig. 15) for the one-way and two-way nesting cases.

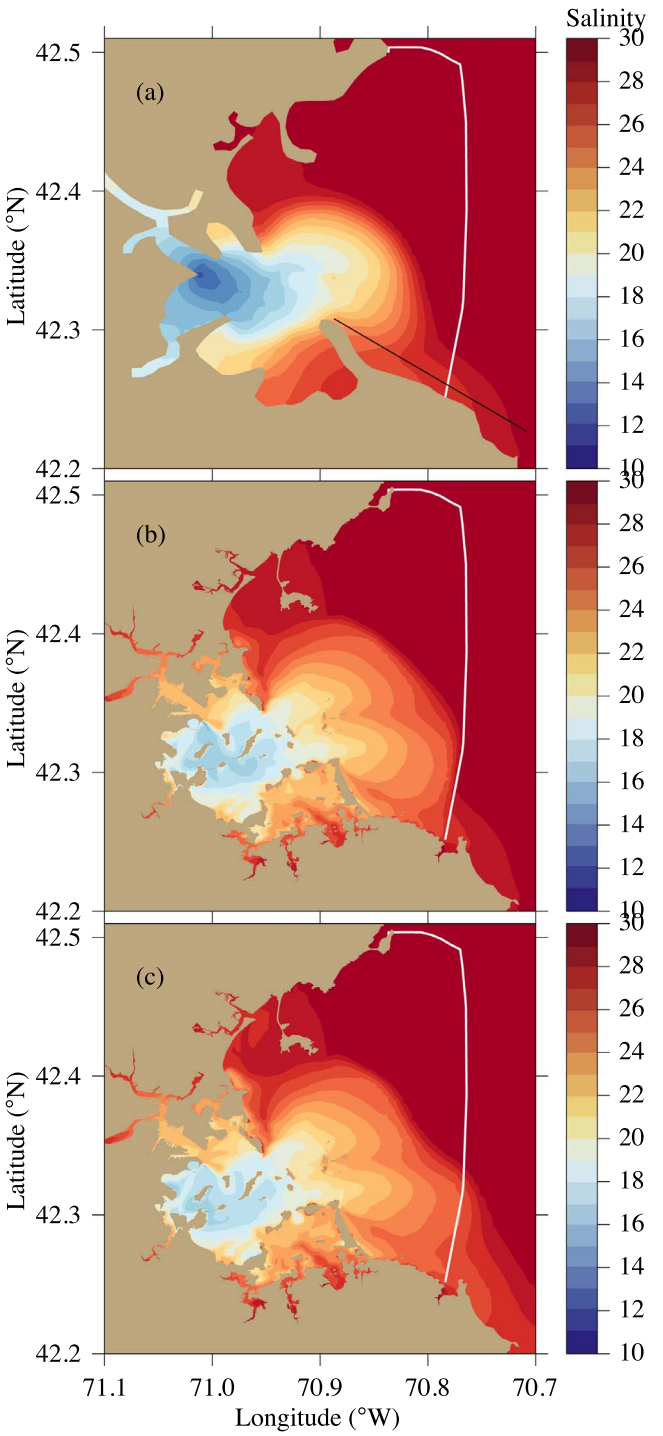

Fig. 18. Comparisons of the distributions of the model-simulated salinity plume in the Boston Harbor region produced by the large-domain model (a), one-way nested model (b) and two-way nested model (c). For the nested model cases, the salinity was drawn by merging the large- and small-domain model results.

based FVCOM. These modules made FVCOM utilize the community coupler for the multi-domain nesting application. With the ESMF, FVCOM can be used to establish a multi-domain nested model system without offline data interpolating and remapping. The ESMF-based two-way nesting method coded in FVCOM was designed with conserved properties in data transition. This approach can efficiently use the supercomputer computational nodes by running larger and smaller domain models simultaneously with boundary conditions exchange.

Experiments were made to evaluate the performance of the one-way and two-way nesting methods. The results not only demonstrated that the nesting methods in FVCOM under the ESMF framework worked well, but also provided us insight into critical issues in selections of one-way and two-way nesting. For storm-induced storm surge application, since the wind-induced flow was onshore, no matter if one-way or two-way nesting was used, the nested model performed well. For a salinity plume case, however, the water movement was featured by an outflow. In this case, the one-way nesting could lead to a water-blocking feature at the nesting boundary, so that two-way nesting should be used.

In general, for a long-term simulation, the two-way nesting should be used to keep the conservative property in the model. For a short-term simulation, the one-way nesting could be used if the nesting boundary was set up in the region far away from the coast. The success

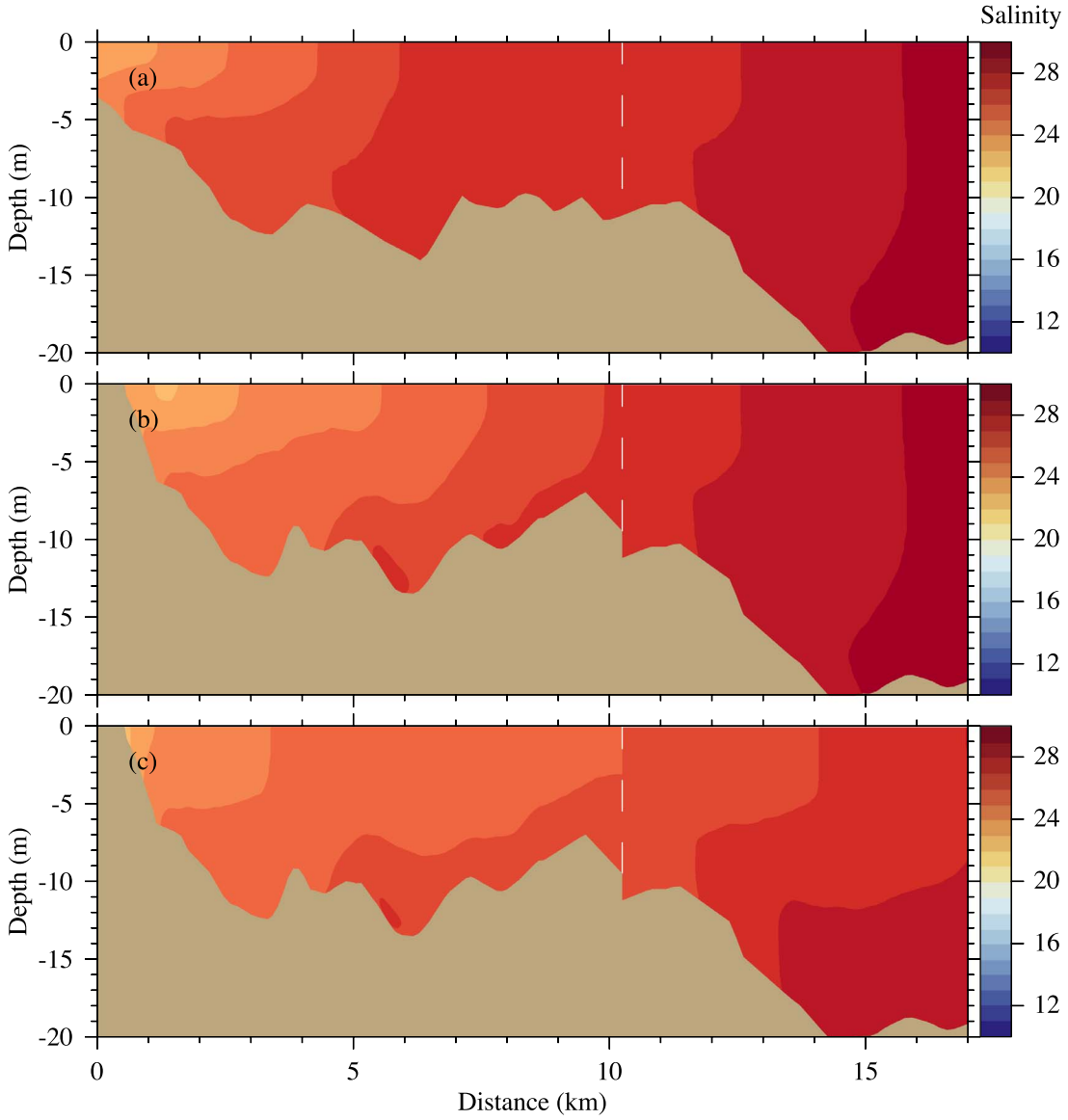

Fig. 19. Vertical distributions of the simulated salinity on the transect shown in Fig. 18a for a) large-domain model run, b) the one-way nested model run and c) the two-way nested model run. For the nested model cases, the salinity was drawn by merging the large- and small-domain model results. The vertical dashed white line in each figure indicates the nesting boundary.

in implementing the ESMF coupler has provided a tool to make FVCOM more applicable to couple with other ocean and meteorological models.

Acknowledgments

This work was supported by the NSF grants OCE1459096, OCE1332207, OCE1332666 and OCE1603000, the MIT Sea Grant College Program through grant 2012-R/RC-127, the NOAA NERACOOS program funds for NECOFS, and the NOAA-CINAR Hurricane Sandy fund. Dr. Chen was also supported by the International Center for Marine Studies at Shanghai Ocean University.

References

Anderson, E.J., Schwab, D.J., 2013. Predicting the oscillating bi-directional exchange flow in the Straits of Mackinac. J. Great Lakes Res. 39 (4), 663–671.

Beardsley, R.C., Chen, C., Xu, Q., 2013. Coastal flooding in Scituate (MA): a FVCOM study of the 27 December 2010 nor'easter. J. Geophys. Res. Oceans 118, 6030–6045. http://dx.doi.org/10.1002/2013JC008862.

Bernholdt, D.E., Allan, B.A., Armstrong, R., Bertrand, F., Chiu, K., Dahlgren, T.L., Damevski, K., Elwasif, W.R., Epperly, T.G.W., Govindaraju, M., Katz, D.S., Kohl, J.A., Krishnan, M., Kumfert, G., Larson, J.W., Lefantzi, S., Lewis, M.J., Malony, A.D., McInnes, L.C., Nieplocha, J., Norris, B., Parker, S.G., Ray, J., Shende, S., Windus, T.L., Zhou, S., 2006. A component architecture for high-performance scientific computing. Int. J. High Perform. C. 20 (2), 163–202.

Bleck, R., 2002. An oceanic general circulation model framed in hybrid isopycnic-Cartesian coordinates. Ocean Modell 4, 55–88.

Burchard, H., 2002. Applied Turbulence Modeling in Marine Waters. Springer, Berlin-Heidelberg-New York-Barcelona-Hong Kong-London-Milan Paris-Tokyo, pp. 215.

Cazenave, P.W., Torres, R., Allen, J.I., 2016. Unstructured grid modelling of offshore wind farm impacts on seasonally stratified shelf seas. Prog. Oceanogr. 145, 25–41. http://dx.doi.org/10.1016/j.pocean.2016.04.004.

Chassignet, E.P., Smith, L.T., Halliwell, G.R., Bleck, R., 2003. North Atlantic simulations with the hybrid coordinate ocean model (HYCOM): impact of the vertical coordinate choice, reference pressure, and thermobaricity. J. Phys. Oceanogr. 33, 2504–2526.

Chassignet, E.P., Hurlburt, H.E., Smedstad, O.M., Halliwell, G.R., Wallcraft, A.J., Metzger, E.J., Blanton, B.O., Lozano, C., Rao, D.B., Hogan, P.J., Srinivasan, A., 2006. Generalized vertical coordinates for eddy-resolving global and coastal ocean forecasts. Oceanography 19 (1), 118–129.

Chen, C., Liu, H., Beardsley, R.C., 2003. An unstructured, finite-volume, three-dimensional, primitive equation ocean model: application to coastal ocean and estuaries. J. Atmos. Oce. Tech. 20, 159–186.

Chen, C., Beardsley, R.C., Cowles, G., 2006. An unstructured grid, finite-volume coastal ocean model (FVCOM) system, special Issue entitled advance in computational oceanography. Oceanography 19 (1), 78–89.

Chen, C., Lai, Z., Beardsley, R.C., Xu, Q., Lin, H., Viet, N.T., 2012. Current separation and upwelling over the southeast shelf of Vietnam in the South China Sea. J. Geophys.

Res. Oceans 117, C03033. http://dx.doi.org/10.1029/2011JC007150.
Chen, C., Beardsley, R.C., Cowles, G., Qi, J., Lai, Z., Gao, G., Stuebe, D., Xu, Q., Xue, P., Ge, J., Hu, S., Ji, R., Tian, R., Huang, H., Wu, L., Lin, H., Sun, Y., Zhao, L., 2013a. An Unstructured Grid, Finite-Volume Community Ocean Model FVCOM User Manual, fourth ed. SMAST/UMASSD Technical Report-13-0701, 404.
Chen, C., Beardsley, R.C., Luettich Jr., R.A., Westerink, J.J., Wang, H., Perrie, W., Xu, Q., Donahue, A.S., Qi, J., Lin, H., Zhao, L., Kerr, P.C., Meng, Y., Toulany, B., 2013b. Extratropical storm inundation testbed: intermodel comparisons in Scituate, Massachusetts. J. Geophys. Res. Oceans 118, 1–20. http://dx.doi.org/10.1002/jgrc.20397.
Chen, C., Beardsley, R.C., 2015. FVCOM: development, improvement and applications. In: Sana, L., Hewawasam, L., Warris, M.B. (Eds.), Proceedings of the Fifth International Conference on Estuaries and Coasts (ICEC), pp. 11–19.
Chen, C., Gao, G., Zhang, Y., Beardsley, R.C., Lai, Z., Qi, J., Lin, H., 2016. Circulation in the Arctic Ocean: Results from a high-resolution coupled ice-sea nested Global-FVCOM and Arctic-FVCOM system. Prog. Oceanogr. 141, 60–80.
Collins, N., Theurich, G., DeLuca, C., Suarez, M., Trayanov, A., Balaji, V., Li, P., Yang, W., Hill, C., da Silva, A., 2005. Design and implementation of components in the earth system modeling framework. Int. J. High Perform. C. 19 (3), 341–350.
Debreu, L., Blayo, E., 2008. Two-way embedding algorithms: a review. Ocean Dyn 58, 415–428.
Debreu, L., Marchesiello, P., Penven, P., Cambon, G., 2012. Two-way nesting in split-explicit ocean models: algorithms, implementation and validation. Ocean Modell 49–50, 1–21.
Dunlap, R., Mark, L., Rugaber, S., Balaji, V., Chastang, J., Cinquini, L., DeLuca, C., Middleton, D., Murphy, S., 2008. Earth system curator: metadata infrastructure for climate modeling. Earth Sci. Inform. 1 (3–4), 131–149. http://dx.doi.org/10.1007/s12145-008-0016-1.
ESMF Joint Specification Team, 2016a. Earth System Modeling Framework ESMF Reference Manual for Fortran Version 7.0.0, 1196 pp.
ESMF Joint Specification Team, 2016b. Earth System Modeling Framework ESMF User Guide Version 7.0.0, 66 pp.
Foreman, M.G.G., Stucchi, D.J., Garver, K.A., Tuele, D., Isaac, J., Grime, T., Guo, M., Morrison, J., 2012. A circulation model for the Discovery Islands, British Columbia. Atmos. Ocean 50 (3), 301–316. http://dx.doi.org/10.1080/07055900.2012.686900.
Fox, A.D., Maskell, S.J., 1995. Two-way interactive nesting of primitive equation ocean models with topography. J. Phys. Oceanogr. 25, 2977–2996.
Hill, C., DeLuca, C., Balaji, V., Suarez, M., da Silva, A., 2004. The architecture of the earth system modeling framework. Comp. Sci. Eng. 6 (1), 18–28.
IPCC, 2007: Climate change 2007. The physical science basis. In: Solomon, S., Qin, D., Manning, M., Chen, Z., Marquis, M., Averyt, K.B., Tignor, M., Miller, H.L. (Eds.), Contribution of Working Group I to the Fourth Assessment Report of the Intergovernmental Panel on Climate Change, Cambridge University Press, Cambridge, United Kingdom and New York, NY, USA, p. 996.
Jacob, R., Larson, J., Ong, E., 2005. MxN communication and parallel interpolation in CCSMV3 using the model coupling toolkit. Int. J. High Perform. C. 19, 293–308.
Kobayashi, M.H., Pereira, J.M.C., Pereira, J.C.F., 1999. A conservative finite-volume second-order-accurate projection method on hybrid unstructured grids. J. Comput. Phys. 150, 40–75.
Lai, Z., Chen, C., Cowles, G., Beardsley, R.C., 2010a. A Non-hydrostatic version of FVCOM, part i: validation experiments. J. Geophys. Res.: Oceans 115. http://dx.doi.org/10.1029/2009 JC005525.
Lai, Z., Chen, C., Cowles, G., Beardsley, R.C., 2010b. A non-hydrostatic version of FVCOM, part ii: mechanistic study of tidally generated nonlinear internal waves in Massachusetts Bay. J. Geophys. Res. Oceans. http://dx.doi.org/10.1029/2010JC006331.
Larson, J., Jacob, R., Ong, E., 2005. The model coupling toolkit, a new fortran90 toolkit for building multiphysics parallel coupled models. Int. J. High Perform. C. 19 (3), 277–292. http://dx.doi.org/10.1177/1094342005056115.
Lin, Y., Fissel, D.B., 2014. High resolution 3-D finite-volume coastal ocean modeling in Lower Campbell River and Discovery Passage, British Columbia, Canada. J. Mar. Sci. Eng 2, 209–225.
Madec, G., Delecluse, P., Imbard, M., Lévy, C., 1998. OPA 8.1 Ocean General Circulation Model reference manual. Note Du Pôle de Modelisation. Institut Pierre-Simon Laplace (IPSL),, France, pp. 91 No 11.
Marshall, J., Hill, C., Perelman, L., Adcroft, A., 1997a. Hydrostatic, quasi-hydrostatic, and nonhydrostatic ocean modeling. J. Geophys. Res. Oceans 102 (C3), 5733–5752.
Marshall, J., Adcroft, A., Hill, C., Perelman, L., Heisey, C., 1997b. A finite-volume, incompressible Navier Stokes model for studies of the ocean on parallel computers. J. Geophys. Res. Oceans 102 (C3), 5753–5766.
McInnes, L.C., Allan, B.A., Armstrong, R., Benson, S.J., Bernholdt, D.E., Dahlgren, T.L., Diachin, L.F., Krishnan, M., Kohl, J.A., Larson, J.W., Lefantzi, S., Nieplocha, J., Norris, B., Parker, S.G., Ray, J., Zhou, S., 2006. Parallel PDE-based simulations using the common component architecture. In: Bruaset, A.M., Bjorstad, P., Tveito (Eds.), Numerical Solution of Partial Differential Equations on Parallel Computers, vol. 51. Springer-Verlag, pp. 327–384 of Lecture Notes in Computational Science and Engineering (LNCSE).
Mellor, G.L., Yamada, T., 1982. Development of a turbulence closure model for geophysical fluid problem. Rev. Geophys. Space. Phys. 20, 851–875.
Pacanowski, R.C., Griffies, S.M., 1999. The MOM3 Manual. Geophysical Fluid Dynamics Laboratory/NOAA. Princeton, USA, pp. 680.
Peng, M., Schmalz, R.A., Zhang, A., Aikman, F., 2014. Towards the development of the national ocean service San Francisco Bay operational forecast system. J. Mar. Sci. Eng. 2, 247–286. http://dx.doi.org/10.3390/jmse2010247.
Pietrzak, J., Jakobson, J.B., Burchard, H., Vested, H.J., Petersen, O., 2002. A three-dimensional hydrostatic model for coastal and ocean modeling using a generalized topography following co-ordinate system. Ocean Modell 4, 173–205.
Qi, J., Chen, C., Beardsley, R.C., Perrie, W., Cowles, G., Lai, Z., 2009. An unstructured-grid finite-volume surface wave model (FVCOM-SWAVE): implementation, validations and applications. Ocean Modell 28, 153–166.
Sheng, J., Greatbatch, R.J., Zhai, X., Tang, L., 2005. A new two-way nesting technique for ocean modelling based on the smoothed semi-prognostic method. Ocean Dyn 55, 162–177.
Smagorinsky, J., 1963. General circulation experiments with the primitive equations, I. The basic experiment. Mon. Weather. Rev. 91, 99–164.
Smith, R.D., 1999. The primitive equations in the stochastic theory of adiabatic stratified turbulence. J. Phys. Oceanogr. 29, 1865–1880.
Wang, D., Harmon, M., Berry, M.W., Carr, E., Gross, L.J., 2011. On design of a coupling component for parallel multimodeling. Int. J. Model. Simul. Sci. Comput. 2 (4), 445–458. http://dx.doi.org/10.1142/S1793962311000554.
Xue, P., Eltahir, E.A.B., 2015. Estimation of the heat and water budgets of the Persian (Arabian) Gulf using a regional climate model. J. Climate 28, 5041–5062. http://dx.doi.org/10.1175/JCLI-D-14-00189.1.
Yang, Z., Richardson, P., Chen, Y., Kelley, J.G.W., Myers, E., Aikman, F., Peng, M., Zhang, A., 2016. Model development and hindcast simulations of NOAA's Gulf of Maine operational forecast system. J. Mar. Sci. Eng. 4 (4), 77. http://dx.doi.org/10.3390/jmse4040077.
Zhang, Y., Chen, C., Beardsley, R.C., Gao, G., Lai, Z., Curry, B., Lee, C.M., Lin, H., Qi, J., Xu, Q., 2016a. Studies of the Canadian Arctic Archipelago water transport and its relationship to basin-local forcings: Results from AO-FVCOM. J. Geophys. Res. Oceans. http://dx.doi.org/10.1002/2016JC011634.
Zhang, Y., Chen, C., Beardsley, R.C., Gao, G., Qi, J., Lin, H., 2016b. Seasonal and interannual variability of the Arctic sea ice: a comparison between AO-FVCOM and observations. J. Geophys. Res. Oceans. http://dx.doi.org/10.1002/2016JC011841.
Zheng, L., Weisberg, R.H., 2012. Modeling the west Florida coastal ocean by downscaling from the deep ocean, across the continental shelf and into the estuaries. Ocean Modell 48, 10–29. http://dx.doi.org/10.1016/j.ocemod.2012.02.002.